Participant Name: Shengdao Ke

School: Phillips Academy Andover

State/Province: MA

Country/Region: USA

Advisor Name: Xianfeng David Gu

Advisor Affiliation:
University of New York at Stony Brook, Stony Brook, 11794, NY, USA

Title of Paper: The Ricci Flow on Trees:
Linear Convergence, Curvature Bounds, and Spectral Applications

Acknowledgements

I would like to express my deepest gratitude to my supervisor, Professor Xianfeng David Gu, for his invaluable guidance throughout the course of my research. I also thank to my family for their unwavering encouragement and understanding during the research journey.

THE RICCI FLOW ON TREES: LINEAR CONVERGENCE, CURVATURE BOUNDS, AND SPECTRAL APPLICATIONS

Abstract. We study Ricci flows on finite weighted trees based on Ollivier-type Ricci curvature, parametrized by an exponent $a \in \mathbb{R}$. For general values of a, we establish uniform bounds on the curvatures and their (weighted) sums. For $a > -1$, we show that all normalized edge weights on internal edges remain uniformly bounded away from zero. In the special case of $a = 0$, the unnormalized Ricci flow can be formulated as a linear ODE, we prove that the normalized flow, starting from any positive initial metric, must converge to a metric with constant curvature. Moreover we can show such metric is unique on each tree. Several bounds for this constant curvature have been established and examples on the double-star graph model demonstrate they can be either positive, zero or negative. We also find from experimental results that, the spectrum of the Ricci flow evolution matrix, comparing to that of other graph matrices, clusters tree structures more effectively.

Keywords: Ricci flow, Ollivier-type Ricci curvature, weighted trees, Einstein metric, spectral clustering, computational experiments

Contents

1. Introduction

Ricci curvature has long played a central role in differential geometry and geometric analysis, most notably through its appearance in Hamilton's pioneering work on the Ricci flow equation [12]

$$\frac{\partial g_{ij}}{\partial t} = -2\,\mathrm{Ric}_{ij},$$

which deforms a Riemannian metric in the direction of its Ricci curvature. Here $g_{ij}(t)$ denotes the components of the evolving Riemannian metric, and Ric_{ij} are the components of its Ricci curvature tensor. Hamilton established short-time existence, uniqueness, and important curvature pinching estimates for the flow [12, 13, 14]. The theory reached its most profound success in Perelman's work [24, 26, 25], where he introduced new monotonicity formulas and the surgery technique, leading to the resolution of the Poincaré conjecture and the more general geometrization conjecture.

In many practical contexts, however, geometric information is available only in discrete or combinatorial form—such as networks, point clouds, or discretized manifolds—so it becomes essential to develop discrete analogues of Ricci flow whose evolution closely approximates the smooth theory. This motivates the study of Ricci flow on graphs, which has advanced significantly in recent years: Weber et al. [29] proposed a geometric method based on the Forman-Ricci flow for change detection in large dynamic datasets, this method analyzes the topological properties of the network, providing a deeper understanding of changes in network structure. Bai et al. [2] established existence and uniqueness of solutions to continuous-time Ricci flow on weighted graphs based on Lin-Lu-Yau Ollivier Ricci curvature. In the study of discrete curvature and Ricci flow, Cushing et al. [4] systematically investigated Ricci flow behavior on graphs via the Bakry–Émery curvature framework. Their work elucidates the interplay between graph structure and curvature evolution, providing valuable insights into how curvature conditions shape graph metrics and dynamics. For the discrete-time Ollivier–Ricci curvature flow on finite weighted graphs, Li and Münch [17] proved that the flow, combined with a surgery procedure, converges to a constant-curvature metric, their proof relies on a convergence result for general nonlinear Markov chains with a monotonicity property.

Discrete Ricci flow has demonstrated strong performance in practical applications: the Ollivier-based flow stretches intercommunity edges and shrinks intracommunity edges, allowing graph partitioning [22]. Ricci curvature–based methods have been used to enhance network alignment by capturing structural similarities between graphs [21]. Curvature-guided graph rewiring mitigates over-squashing and improves message passing in GNNs [28]. Other Ricci-type flows study various aspects of graph geometry and dynamics [10, 3, 9, 16, 30, 7, 11, 5, 8, 6, 31, 15]. These developments illustrate the growing interplay between discrete network geometry and classical geometric analysis.

In this work, we study a general form of Ollivier-type Ricci curvature on finite weighted trees, parameterized by a real exponent $a \in \mathbb{R}$. The curvature is defined via local probability distributions μ_x^α, where a portion α of the mass remains at vertex x, and the remaining mass $1-\alpha$ is distributed among neighbors proportionally to $P_{xy} = w_{xy}^a$, a power of the edge weights. This framework preserves desirable properties such as invariance under metric scaling and allows for flexible modeling of transport dynamics on graphs.

We focus on the associated *Ricci flow*, a geometric evolution equation that adjusts the edge weights over time based on curvature. In [2], the authors introduced the *unnormalized* and *normalized* Ricci flow defined on graphs. Given an undirected graph G with a positive initial weight function w_0, an un-normalized Ricci flow is the evolution of the weight function $w = w(t)$ satisfying following system of ordinary equations:

$$\begin{cases} w(0) = w_0, \\ \frac{\partial w_e(t)}{\partial t} = -\kappa_e(t) w_e(t), \text{ for all } e \in E(G), \end{cases} \tag{1}$$

where $\kappa_e(t)$ represents the Lin-Lu-Yau Ollivier Ricci curvature on edge e at time t. This system of equations, captures the dynamic evolution of the metric (edge weights) on a graph over time. The curvatures $\kappa_e(t)$ influence the rate of change of the edge weights $w_e(t)$, with a negative curvature leading to an increase in weight and a positive curvature leading to a decrease. This behavior aligns with the intuitive understanding of Ricci flow, where negative curvature tends to "expand" the geometry while positive curvature tends to "shrink" it.

The normalized Ricci flow on graphs, which adjusts the total edge weights to remain constant 1, is described by the following system of equations

$$\frac{\partial w_e(t)}{\partial t} = -\kappa_e(t) w_e(t) + w_e \sum_{h \in E(G)} \kappa_h w_h(t), \tag{2}$$

where $w_e(t)$ represents the normalized weight of edge e at time t. In [2], the author established conditions for the long time existence and uniqueness of global solutions to Ricci flows on general graphs.

For trees, their combinatorial simplicity enables the explicit computation of the Lin-Lu-Yau Ollivier Ricci curvature on any two vertices u, v:

$$\kappa_{uv} = -\frac{\sum\limits_{x \sim u} w_{ux}^{1+a}}{w_{uv} \sum\limits_{x \sim u} w_{ux}^{a}} + 2 \cdot \frac{w_{uv}^{a}}{\sum\limits_{x \sim u} w_{ux}^{a}} + 2 \cdot \frac{w_{uv}^{a}}{\sum\limits_{y \sim v} w_{vy}^{a}} - \frac{\sum\limits_{y \sim v} w_{vy}^{1+a}}{w_{uv} \sum\limits_{y \sim v} w_{vy}^{a}}. \tag{3}$$

The parameter a, originating from the probability distributions, plays a crucial role, as it affects both the analytical approach and the resulting behavior of the Ricci flow.

We say that a solution to the Ricci flow *converges* if, for every edge $h \in E$, the limit of *the normalized weight* $w_h(t)$ exists. The function $w(\infty)$ obtained in this way is called the *limit metric*. It is also important to study the static solution of the normalized Ricci flow. Such metric satisfies:

$$\kappa_e = \kappa \quad \text{for every edge } e,$$

and will be called *a metric of constant curvature* or *an Einstein metric*. It is easy to see the sign of the constant κ determines the unnormalized flow of such metric is expanding, static or shrinking.

In this work, we investigate the long-time behavior of the solution to the Ricci flow. We focus on the case $a = 0$, where we establish sharp bounds for the limiting curvature and prove that the normalized Ricci flow converges to the unique metric of constant curvature on the tree.

Our contributions are summarized as follows: We derive an explicit formula for the generalized Ricci curvature equation (3) in terms of the edge weights and the parameter a on a tree, and analyze its qualitative behavior.

Proposition 1. *Let $T = (V, E)$ be a tree, and let κ_{uv} be the curvature in (3) with $a \in \mathbb{R}$. Then the sum of the Lin-Lu-Yau Ollivier Ricci curvature on all edges satisfies:*

$$\sum_{uv\in E} \kappa_{uv} \begin{cases} \leq 2, & a > -1, \\ = 2, & a = -1, \\ \in [2, \, |V|], & a < -1. \end{cases}$$

Moreover, for all $a \in \mathbb{R}$,

$$\kappa_{uv} \leq 2$$

and for $a \leq -1$ we have the uniform bound

$$-2(|V| - 3) \leq \kappa_{uv} \leq 2.$$

Moreover, the curvature bounds play a crucial role in preventing local degeneracy of the edge weights. When $a > -1$, we show that all normalized weights on internal edges remain uniformly bounded away from zero. This result will be established in Proposition 5.

In the special case of $a = 0$, the probability distribution μ_x^α in the definition of Ollivier Ricci curvature (see Definition 2) is defined in the following way:

$$\mu_x^\alpha(y) = \begin{cases} \alpha, & \text{if } y = x, \\ (1-\alpha)\frac{1}{d_x}, & \text{if } y \sim x, \\ 0, & \text{otherwise.} \end{cases}$$

This distribution μ_x^α describes a simple model of local movement or diffusion: With probability α, a particle (or agent) at node x stays in place. With probability $1-\alpha$, it moves to one of its neighbors, choosing *uniformly at random* among the d_x neighbors. This is referred to as the equal probability model because the probabilities of moving to any neighbors are the same. Such a model applies to various real-world systems, for example: A tourist at location x who either stays with probability α or chooses a neighboring street at random to walk to; A data packet in a network that routes randomly to a connected node; An idea or infection that spreads randomly from one individual to their direct contacts. Intuitively, using equal probability movement simplifies the model and reflects unbiased local diffusion, making it useful for studying the geometric and transport properties of graphs.

The (unnormalized) Ricci flow on a weighted tree $T = (V, E, w)$ in this special case reads:

$$\frac{\partial}{\partial t} w_{xy}(t) = -\left(\frac{1}{d_x} + \frac{1}{d_y}\right) w_{xy}(t) + \frac{1}{d_x} \sum_{u\sim x, \; u\neq y} w_{xu}(t) + \frac{1}{d_y} \sum_{v\sim y, \; v\neq x} w_{vy}(t), \qquad (4)$$

where d_x represent the degree of vertex x. Note that the flow equation is linear with the coefficient matrix $R \in \mathbb{R}^{|E|\times|E|}$, which we shall call *the evolution matrix* of the tree. For such flow, we have established the following result:

Theorem 1 (Convergence of Ricci Flow on Weighted Trees)**.** *Let $T = (V, E, w_0)$ be a finite, weighted tree with edge weights being strictly positive. Let $w = w(t)$ be the Ricci flow (4) on T with initial weight w_0.*

(1) ***(Long time existence)*** *The solution $w = w(t)$ exists uniquely for any positive initial metric and for all time $t > 0$. Under the flow, $w_e(t) > 0$ for all $t > 0$ and $e \in E$.*
(2) ***(Convergence to equilibrium)*** *The normalized Ricci flow converges to an Einstein metric $w(\infty)$ with curvature $\kappa(\infty)$. In particular, a tree $T = (V, E)$ always admits an Einstein metric in sense of* (21)*.*
(3) ***(Limit behavior)*** *The limit curvature κ_∞ is equal to the negative of the largest eigenvalue of the evolution matrix associated with the Ricci flow*

In this theorem, we employ a flow method to establish the existence of an Einstein metric on a tree. Moreover, one can show that, for a given tree, such Einstein metric is unique (also see Proposition 6)

Proposition 2. *Let $T = (V, E)$ be a tree, and $w, w' \in \mathbb{R}_+^E$ be two (normalized) metrics on T with constant curvatures κ and κ', then $w = w'$ and $\kappa = \kappa'$.*

Therefore, one may expect that the Einstein metric w and its curvature κ capture important structural information about the tree. In what follows, we provide upper and lower bounds for the curvature κ. Both bounds are expressed in terms of combinatorial data of the tree, and each is attained only when the tree is a star.

Proposition 3. *Let κ be the curvature of the Einstein metric. Then:*

$$2 \min_{xy\in E} \left(\frac{1}{d_x} + \frac{1}{d_y} - 1 \right) \le \kappa \le \frac{2}{|E|}. \tag{5}$$

Any one of the equalities holds if and only if T is a star graph.

Besides, we also establish a path-wise identity for Einstein metrics on trees, which constrains feasible weight assignments and provides insight into how local curvature conditions propagate along the tree.

Proposition 4 (Alternating Sum Identity on Path of all Trees)**.** *Let $T = (V, E, w)$ be a finite weighted tree with positive edge weights $w : E \to \mathbb{R}_{>0}$. Assume w is the Einstein metric.*

Let $P = (v_0, v_1, \ldots, v_k)$ be a path in the tree, with corresponding edges $e_i = v_{i-1}v_i$ for $i = 1, \ldots, k$ where v_0 and v_k are leaf nodes, then we have

$$\sum_{i=1}^{k} (-1)^{i-1} \kappa \cdot w_{e_i} = -w_{e_1} + (-1)^k w_{e_k} + \sum_{i=1}^{k} (-1)^{i-1} \left(\frac{2}{d_{v_{i-1}}} + \frac{2}{d_{v_i}} \right) w_{e_i}.$$

Although the present work focuses on the theoretical analysis of Ricci flow on trees, these results provide a foundational framework for studying Ricci flow on more general graphs. Tree-structured data occur naturally in many domains, including natural language processing (NLP), where constituency and dependency trees [20, 23] serve as hierarchical sentence representations. Recursive neural networks (RecNNs) [27, 18] exploit such trees to encode syntactic and semantic information for tasks such as sentiment analysis, semantic parsing, and question answering. These connections underscore the potential relevance of theoretical insights on Ricci flow for tree structures to broader applications.

Building on our theoretical results for Ricci flow, we show that the spectrum of the Ricci flow-based *Evolution Matrix* R effectively clusters tree structures, outperforming classical adjacency, Laplacian, and distance matrices. The matrix is sparse, curvature-aware, and interpretable, demonstrating how discrete Ricci flow offers both a principled framework and practical analytical tools.

Organization of the Paper. The rest of this paper is arranged in a straightforward way. In Section 2, we go over some basic ideas about trees and Ricci curvature. In Section 3, we explain how Ricci curvature works on trees. Section 4 looks at the Ricci flow when $a = 0$ and shows how the flow behaves in the long run, ending with Theorem 1. In Section 5, we introduce the Ricci flow "Evolution Matrix" on trees and show how it can be used to get spectral features and to cluster different trees. Finally, Section 6 talks about a possible direction for future work, where we guess that the largest eigenvalue and eigenvector of the Ricci flow matrix might actually determine a finite tree completely.

2. Preliminaries and Definitions

Let $G = (V, E)$ be a finite, undirected graph without loops or multiple edges. The edge weight can be viewed as a function $w : E \to (0, \infty)$ which assigns a positive weight to each edge $e \in E$, and the triple $G = (V, E, w)$ is called a weighted graph. We say that G is a *metric graph* if for every pair of adjacent vertices $x, y \in V$, the weight of the edge equals the distance:

$$x \sim y \quad \Rightarrow \quad d(x, y) = w_{xy}.$$

A path in G is called a weighted path if each edge on the path has nonzero weight. The graph G is said to be connected if every pair of vertices is connected by a weighted path. For any two vertices $x, y \in V$, we write $x \sim y$ if $\{x, y\} \in E$. The *distance* between two vertices $x, y \in V$, denoted by $d(x, y)$, is defined as the minimum total distance among all paths connecting x and y. That is,

$$d(x, y) := \min_{\text{paths } P \text{ from } x \text{ to } y} \sum_{\{u,v\} \in P} d(u, v),$$

where the sum is over the edges $\{u, v\}$ in the path P.

For any vertex $x \in V$, let $N(x)$ denote the set of its neighbors, and define the degree of x by $d_x = |N(x)|$. Usually, we use n to denote the number of vertices, and m to denote the number of edges.

Definition 1 (Coupling and Transportation Distance)**.** *Let V be a finite set, and let μ_1 and μ_2 be two probability distributions on V.*

A coupling *of μ_1 and μ_2 is a new probability distribution $\pi(x, y)$ defined on the product space $V \times V$, representing a plan for moving mass from x to y. The coupling must satisfy:*

$$\sum_{y \in V} \pi(x, y) = \mu_1(x), \quad \sum_{x \in V} \pi(x, y) = \mu_2(y).$$

This means that the total mass transported out of point x equals $\mu_1(x)$, and the total mass transported into point y equals $\mu_2(y)$.

Given a distance function $d(x, y)$ on V, the transportation distance *(also called the* Wasserstein-1 distance*) between μ_1 and μ_2 is defined as:*

$$W(\mu_1, \mu_2) := \inf_{\pi} \sum_{x,y \in V} \pi(x, y) \cdot d(x, y),$$

where the infimum is taken over all valid couplings π.

There is another, equivalent way to express the transportation distance, using an optimization over functions:

$$W(\mu_1, \mu_2) = \sup_{f} \sum_{x \in V} f(x) \left[\mu_1(x) - \mu_2(x)\right],$$

where the supremum is taken over all functions $f : V \to \mathbb{R}$ that satisfy the *1-Lipschitz condition*:

$$|f(x) - f(y)| \leq d(x, y), \quad \text{for all } x, y \in V.$$

Example 1. *Let T be a weighted tree with set of vertices $V = \{1, 2, 3, 4, 5\}$ and edges:*

$$\{12, \quad 23, \quad 24, \quad 45\}$$

where each edge has length/weight one. Consider two probability distributions supported on V:

$$\mu_1 = (0.5,\ 0,\ 0.3,\ 0.2,\ 0), \quad \mu_2 = (0,\ 0.4,\ 0.2,\ 0,\ 0.4)$$

One possible transportation plan from μ_1 to μ_2 can be:

Source $\to$ Target	*Mass*	*Distance*	*Contribution*
$1 \to 2$	0.4	1	0.4
$1 \to 5$	0.1	3	0.3
$3 \to 3$	0.2	0	0
$3 \to 2$	0.1	1	0.1
$4 \to 5$	0.2	1	0.2

Therefore the cost for this transportation is:

$$C(\mu_1, \mu_2) = 0.4 + 0.3 + 0 + 0.1 + 0.2 = 1$$

To see this transportation plan is optimum, we choose a 1-Lipschitz function $f : V \to \mathbb{R}$ with:

$$f(1) = 0, \quad f(2) = -1, \quad f(3) = -1, \quad f(4) = -2, \quad f(5) = -3.$$

From the point view of the duality, the following quantity gives an upper bound for the Wasserstein distance $W(\mu_1, \mu_2)$:

$$\begin{aligned}\sum_{x\in V} f(x)\big[\mu_1(x) - \mu_2(x)\big] &= 0\cdot 0.5 - 1\cdot(-0.4) - 2\cdot(0.3-0.2) - 2\cdot 0.2 - 3\cdot(-0.4)\\ &= 0.4 - 0.2 - 0.4 + 1.2\\ &= 1.\end{aligned}$$

Therefore, we conclude the plan showed in the table is optimum and the Wasserstein distance of two distributions is:

$$W(\mu_1, \mu_2) = 1.$$

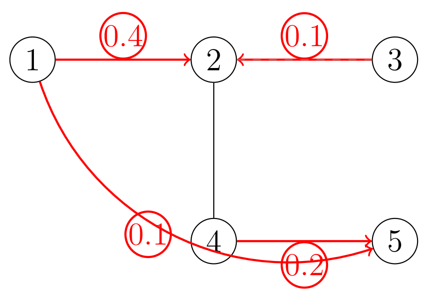

FIGURE 1. Transportation plan $\pi(x, y)$ with curved arrow for long-distance transport (1→5). Red arrows indicate mass movement.

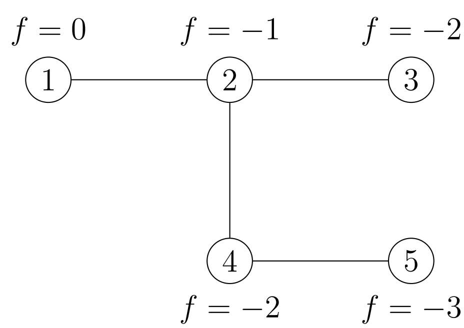

FIGURE 2. 1-Lipschitz function f shown outside the vertex circles.

2.1. **Ollivier-type Ricci Curvature.** Let $\alpha \in [0,1]$ and let $x \in V$ be a vertex. Define a probability distribution μ_x^α on V by

$$\mu_x^\alpha(y) = \begin{cases} \alpha, & \text{if } y = x,\\ (1-\alpha)\dfrac{P_{xy}}{\sum\limits_{z\sim x} P_{xz}}, & \text{if } y \sim x,\\ 0, & \text{otherwise,}\end{cases}$$

where $P : E \to [0,1]$ is a nonnegative function representing the raw probability of moving from vertex x to a neighbor y. The values P_{xy} may depend on the edge weights w_{xy}, and they determine how the total mass $1-\alpha$ is distributed among the neighbors of x. A natural choice for P, especially when w_{uv} represents edge length or cost, is

$$P_{uv} = w_{uv}^a,$$

for some exponent $a \in \mathbb{R}$. This form ensures compatibility with scaling properties of the metric: if all edge weights are scaled by a common factor (i.e., $w_{uv} \mapsto \lambda w_{uv}$), then the distribution of mass remains consistent under appropriate choice of a. This property is essential for deriving the normalized Ricci flow equations.

Definition 2. [19] *Given local probability distribution μ_x^α for every vertex, the α-*Ricci curvature *between two adjacent vertices $x \sim y$ is defined as*

$$\kappa_\alpha(x,y) := 1 - \frac{W(\mu_x^\alpha, \mu_y^\alpha)}{d(x,y)}, \tag{6}$$

where $W(\mu_x^\alpha, \mu_y^\alpha)$ denotes the transportation distance between μ_x^α and μ_y^α, and $d(x,y)$ is the distance between x and y.

Finally, the (Lin–Lu–Yau) Ricci curvature *is defined as the negative derivative of $\kappa_\alpha(x,y)$ at $\alpha = 1$:*

$$\kappa_{xy} := \lim_{\alpha \to 1} \frac{\kappa_\alpha(x,y)}{1-\alpha}. \tag{7}$$

This limit captures the infinitesimal behavior of the curvature as the probability distribution becomes increasingly concentrated at each vertex.

2.2. **The Ricci Flow Equations.** The unnormalized continuous Ricci flow on a graph is defined by the time evolution of the edge weights $w_{xy}(t)$, governed by the system:

$$\frac{\partial w_{xy}(t)}{\partial t} = -\kappa_{xy}(t) \cdot w_{xy}(t), \quad w(0) \in \mathbb{R}^m > 0, \tag{8}$$

where $w(0) = \langle w_{e_1}(0), w_{e_2}(0), \ldots, w_{e_m}(0) \rangle$ is the vector of initial edge weights, and each $w_{e_i}(0)$ represents the initial weight assigned to edge e_i.

Assuming the initial total weight satisfies $\sum_{e \in E} w_e(0) = 1$, the normalized continuous Ricci flow on the graph is governed by the system

$$\frac{\partial w_{xy}(t)}{\partial t} = -\kappa_{xy}(t) \cdot w_{xy}(t) + w_{xy}(t) \sum_{e \in E} \kappa_e(t) w_e(t), \quad w(0) \in R^m > 0, \tag{9}$$

where the normalization ensures that $\sum_{e \in E} w_e(t) = 1$ for all t.

In both equations, $\kappa_{uv}(t)$ is the Ricci curvature at time t, and $w_{uv}(t)$ is the evolving edge weight. Note that the normalized weights (solution to (9)) is also obtained from the unnormalized weight (solution to (8)):

$$\tilde{w}_e(t) = \frac{w_e(t)}{\sum_{e' \in E} w_{e'}(t)}.$$

Analogous to the smooth Ricci flow in differential geometry, the Ricci flow (8) contracts edges with positive curvature and expands those with negative curvature. Specifically, this means: If $\kappa_{uv}(t) > 0$, the edge (u, v) contracts, and the weight $w_{uv}(t)$ decreases. If $\kappa_{uv}(t) < 0$, the edge (u, v) expands, and the weight $w_{uv}(t)$ increases. If $\kappa_{uv}(t) = 0$, the edge weight $w_{uv}(t)$ remains constant. Since κ_{uv} depends on the weights w_{uv} (via $P_{uv} = w_{uv}^a$), this creates a nonlinear feedback loop: curvature affects weights, and weights in turn reshape the curvature.

3. Ricci Curvatures on Trees

In this section, we derive an explicit expression for the Ollivier-type Ricci curvature on trees under the general mass transport model defined earlier.

Let $x \sim y$ be two adjacent vertices in a finite tree $T = (V, E, w)$, with positive edge weights $w_{xy} > 0$. Let the probability of mass transport be given by $P_{xy} = w_{xy}^a$ for some exponent $a \in \mathbb{R}$, and define:

$$P_x^{(a)} := \sum_{z \sim x} P_{xz} = \sum_{z \sim x} w_{xz}^a.$$

We consider the probability measure μ_x^α supported in the neighbourhood of x as:

$$\mu_x^\alpha(z) = \begin{cases} \alpha, & \text{if } x = x, \\ (1-\alpha)\dfrac{w_{xz}^a}{P_x^{(a)}}, & \text{if } z \sim x, \\ 0, & \text{otherwise.} \end{cases}$$

By adapting the results of Theorem 2.10 in [1], we have the following for trees:

Lemma 1. *Let $T = (V, E, d, w)$ be a weighted tree, and let $x \sim y$ be adjacent nodes with $P_x^{(a)} \geq P_y^{(a)}$. For any*

$$\alpha \in \Big(\frac{w_{xy}^a}{w_{xy}^a + P_x^{(a)}},\ 1 \Big],$$

the map $\alpha \mapsto \kappa_\alpha(x, y)$ is linear on the interval

$$\Big[\frac{w_{xy}^a}{w_{xy}^a + P_x^{(a)}},\ 1 \Big].$$

Remark 1. *For trees, Lemma 1 implies that the function $\alpha \mapsto \kappa_\alpha(x, y)$ is linear on $\big[\frac{w_{xy}^a}{w_{xy}^a + P_x^{(a)}}, 1\big]$. Consequently, in applications, it is sufficient to evaluate κ_{xy} at any α sufficiently close to 1 (e.g., $\alpha = 0.99$).*

Since there is a unique path between two vertices in a tree, we can find the explicit formula for κ_{xy} in this setting.

Lemma 2. *Let $T = (V, E, w)$ be a tree where w represents the weight on the edges E. Then for every edge $xy \in E$, the Lin-Lu-Yau Ollivier curvature κ_{xy} is determined by* *the following equation:*

$$\kappa_{xy} = -\sum_{z\sim x}\frac{w_{xz}^{a+1}}{w_{xy}P_x^{(a)}} + 2\frac{w_{xy}^a}{P_x^{(a)}} + 2\frac{w_{xy}^a}{P_y^{(a)}} - \sum_{z\sim y}\frac{w_{yz}^{a+1}}{w_{xy}P_y^{(a)}} \tag{10}$$

Proof. Note that w_{xy} on tree is equal to the distance $d(x,y)$. By Remark 1, we can take α with $1-\alpha$ being small for computing κ_{xy}.

The optimum coupling/distribution π to compute the Wasserstein distance between μ_x and μ_y can be chosen as:

- for each $u \sim x$ and $u \neq y$, $\pi(u,x) = (1-\alpha)\frac{w_{xu}^a}{P_x^{(a)}}$ and for each $v \sim y$ and $v \neq x$, $\pi(y,v) = (1-\alpha)\frac{w_{yv}^a}{P_y^{(a)}}$;
- $\pi(x,y) = \alpha + (1-\alpha)\sum_{z\sim x, z\neq y}\frac{w_{xz}^a}{P_x^{(a)}} - (1-\alpha)\frac{w_{xy}^a}{P_y^{(a)}} > 0$ when α is close to 1;
- for other pair of vertices $u,\ v,\ \pi(u,v)$ takes zero.

Then according to Definition 1, the distance can be computed as

$$W(\mu_x^\alpha,\mu_y^\alpha) = \sum_{z\sim x, z\neq y}(1-\alpha)\frac{w_{xz}^a}{P_x^{(a)}}w_{xz} + \left(\alpha + (1-\alpha)\sum_{z\sim x, z\neq y}\frac{w_{xz}^a}{P_x^{(a)}} - (1-\alpha)\frac{w_{xy}^a}{P_y^{(a)}}\right)w_{xy} + \sum_{z\sim y, z\neq x}(1-\alpha)\frac{w_{yz}^a}{P_y^{(a)}}w_{yz}$$

It follows that

$$\frac{W(\mu_x^\alpha,\mu_y^\alpha)}{w_{xy}} = (1-\alpha)\sum_{z\sim x, z\neq y}\frac{w_{xz}^a}{P_x^{(a)}}\frac{w_{xz}}{w_{xy}} + \alpha + (1-\alpha)\sum_{z\sim x, z\neq y}\frac{w_{xz}^a}{P_x^{(a)}} - (1-\alpha)\frac{w_{xy}^a}{P_y^{(a)}} + (1-\alpha)\sum_{z\sim y, z\neq x}\frac{w_{yz}^a}{P_y^{(a)}}\frac{w_{yz}}{w_{xy}}$$

The α-Ricci curvature (6) is then given by:

$$1 - \frac{W(\mu_x^\alpha,\mu_y^\alpha)}{w_{xy}} = (1-\alpha)\left(1 - \sum_{z\sim x, z\neq y}\frac{w_{xz}^a}{P_x^{(a)}}\frac{w_{xz}}{w_{xy}} - \sum_{z\sim x, z\neq y}\frac{w_{xz}^a}{P_x^{(a)}} + \frac{w_{xy}^a}{P_y^{(a)}} - \sum_{z\sim y, z\neq x}\frac{w_{yz}^a}{P_y^{(a)}}\frac{w_{yz}}{w_{xy}}\right).$$

Using $P_x^{(a)} = \sum_{z\sim x} w_{xz}^a$ and $1 - \sum_{z\sim x, z\neq y}\frac{w_{xz}^a}{P_x^{(a)}} = \frac{w_{xy}^a}{P_x^{(a)}}$, then we have

$$\frac{\kappa_\alpha(x,y)}{1-\alpha} = -\sum_{z\sim x, z\neq y}\frac{w_{xz}^a}{P_x^{(a)}}\frac{w_{xz}}{w_{xy}} + \frac{w_{xy}^a}{P_x^{(a)}} + \frac{w_{xy}^a}{P_y^{(a)}} - \sum_{z\sim y, z\neq x}\frac{w_{yz}^a}{P_y^{(a)}}\frac{w_{yz}}{w_{xy}}$$

Finally, the Lin-Lu-Yau Ollivier Ricci curvature (7) is given by

$$\begin{aligned}\kappa_{xy} = \lim_{\alpha\to 1}\frac{\kappa_\alpha(x,y)}{1-\alpha} &= -\sum_{z\sim x, z\neq y}\frac{w_{xz}^{a+1}}{w_{xy}P_x^{(a)}} + \frac{w_{xy}^a}{P_x^{(a)}} + \frac{w_{xy}^a}{P_y^{(a)}} - \sum_{z\sim y, z\neq x}\frac{w_{yz}^{a+1}}{w_{xy}P_y^{(a)}} \\ &= -\sum_{z\sim x}\frac{w_{xz}^{a+1}}{w_{xy}P_x^{(a)}} + 2\frac{w_{xy}^a}{P_x^{(a)}} + 2\frac{w_{xy}^a}{P_y^{(a)}} - \sum_{z\sim y}\frac{w_{yz}^{a+1}}{w_{xy}P_y^{(a)}}.\end{aligned}$$

$\square$

3.1. **Bounds of Curvature for General** a**.** In this subsection, we derive bounds for terms appearing in the Ricci flow equations such as the Ricci curvature and its product with the normalized edge weights.

Lemma 3. *Let* $T = (V, E, w)$ *be a tree where* w *represents a normalized weight function on the edges* E*. Then for every edge* $uv \in E$*, the following hold:*

(1) $\kappa_{uv} \leq 2$ *and* $\kappa_{uv} w_{uv} \geq -2$*;*

(2) $\left|\sum_{uv\in E} \kappa_{uv} w_{uv}\right| \leq \sum_{u\in V} |2 - d_u|$.

Proof of (1). For each edge $uv \in E(G)$, to derive the upper bound of k_{uv}, it suffices to notice

$$\kappa_{uv} = \frac{2w_{uv}^{a+1} - \sum\limits_{x\sim u} w_{ux}^{1+a}}{w_{uv} \sum\limits_{x\sim u} w_{ux}^{a}} + \frac{2w_{uv}^{a+1} - \sum\limits_{y\sim v} w_{vy}^{1+a}}{w_{uv} \sum\limits_{y\sim v} w_{vy}^{a}} \leq 2,$$

with equality held iff uv is the unique edge of the tree. For the lower bound of $\kappa_{uv} w_{uv}$, we rewrite the term $\kappa_{uv} w_{uv}$ as:

$$\kappa_{uv} w_{uv} = \frac{2}{P_u^{(a)}} \cdot w_{uv}^{a+1} + \frac{2}{P_v^{(a)}} \cdot w_{uv}^{a+1} - \frac{P_u^{(a+1)}}{P_u^{(a)}} - \frac{P_v^{(a+1)}}{P_v^{(a)}}, \tag{11}$$

Since $0 \leq w_{uv} \leq 1$, then $0 \leq P_x^{(a+1)} \leq P_x^{(a)}$ and we obtain the lower bound:

$$\kappa_{uv} w_{uv} \geq \frac{2}{P_u^{(a)}} \cdot w_{uv}^{a+1} + \frac{2}{P_v^{(a)}} \cdot w_{uv}^{a+1} - 2 \geq -2.$$

$\square$

Proof of (2). Using (11), it is easy to see:

$$\begin{aligned}
\sum_{uv\in E} \kappa_{uv} w_{uv} &= \sum_{u\in V} \frac{2}{P_u^{(a)}} \sum_{v\sim u} w_{uv}^{a+1} - \sum_{u\in V} \frac{P_u^{(a+1)}}{P_u^{(a)}} \sum_{v\sim u} 1 \\
&= \sum_{u\in V} \frac{2}{P_u^{(a)}} \cdot P_u^{a+1} - \sum_{u\in V} \frac{P_u^{(a+1)}}{P_u^{(a)}} \cdot d_u \\
&= \sum_{u\in V} (2 - d_u) \cdot \frac{P_u^{(a+1)}}{P_u^{(a)}}.
\end{aligned} \tag{12}$$

Therefore, we can conclude:

$$\left|\sum_{uv\in E} \kappa_{uv} w_{uv}\right| \leq \sum_{u\in V} |2 - d_u| \cdot \frac{P_u^{(a+1)}}{P_u^{(a)}} \leq \sum_{u\in V} |2 - d_u|.$$

$\square$

Similarly, we can write the curvature k_{uv} as:

$$\kappa_{uv} = \frac{2}{P_u^{(a)}} \cdot w_{uv}^a + \frac{2}{P_v^{(a)}} \cdot w_{uv}^a - \frac{P_u^{(a+1)}}{P_u^{(a)}} \cdot w_{uv}^{-1} - \frac{P_v^{(a+1)}}{P_v^{(a)}} \cdot w_{uv}^{-1}. \tag{13}$$

It then follows that

$$\begin{aligned} \sum_{uv\in E} \kappa_{uv} &= \sum_{u\in V} \frac{2}{P_u^{(a)}} \sum_{v\sim u} w_{uv}^a - \sum_{u\in V} \frac{P_u^{(a+1)}}{P_u^{(a)}} \sum_{v\sim u} w_{uv}^{-1} \\ &= \sum_{u\in V} \left(2 - \frac{P_u^{(a+1)} P_u^{(-1)}}{P_u^{(a)}}\right). \end{aligned} \tag{14}$$

Using $P_u^{(a+1)} P_u^{(-1)} \geq P_u^{(a)}$, we can deduce

$$\sum_{uv\in E} \kappa_{uv} \leq \sum_{u\in V} (2-1) = |V|.$$

Note when $a = -1$, from Equation 14,

$$\sum_{uv\in E} \kappa_{uv} = \sum_{u\in V} (2 - P_u^{(0)}) = \sum_{u\in V} (2 - d_u) = 2.$$

3.2. **Proof of Proposition 1.** To give a more tight estimate of the sum of Ricci curvatures and give a proof of Proposition 1 , we shall use the following lemma:

Lemma 4. *For each $u \in V(G)$, the function $h_u(a) := \frac{P_u^{(a)}}{P_u^{(a+1)}}$ is decreasing in $\mathbb{R}$.*

Proof. Let $u \in V(G)$ and denote $w_i := w_{ux}$ for each neighbor $x \sim u$. Recall that

$$h_u(a) := \frac{P_u^{(a)}}{P_u^{(a+1)}} = \frac{\sum_i w_i^a}{\sum_i w_i^{a+1}}.$$

To show that $h_u(a)$ is decreasing, take any $b > a$. It suffices to show

$$h_u(a) \geq h_u(b) \quad \Longleftrightarrow \quad P_u^{(b+1)} P_u^{(a)} - P_u^{(a+1)} P_u^{(b)} \geq 0.$$

Compute:

$$\begin{aligned} P_u^{(b+1)} P_u^{(a)} - P_u^{(a+1)} P_u^{(b)} &= \sum_i \sum_j \left(w_i^{b+1} w_j^a - w_i^b w_j^{a+1}\right) \\ &= \sum_i \sum_j w_i^b w_j^a (w_i - w_j) \\ &= \frac{1}{2} \sum_i \sum_j \left[w_i^b w_j^a (w_i - w_j) + w_j^b w_i^a (w_j - w_i)\right] \\ &= \frac{1}{2} \sum_i \sum_j w_i^a w_j^a \left(w_i^{b-a} - w_j^{b-a}\right)(w_i - w_j). \end{aligned}$$

Since $b - a > 0$, the function $x \mapsto x^{b-a}$ is increasing, so

$$(w_i^{b-a} - w_j^{b-a})(w_i - w_j) \geq 0 \text{ for all } i, j, \text{ and } w_i^a w_j^a \geq 0.$$

Therefore, the sum is nonnegative:

$$P_u^{(b+1)}P_u^{(a)} - P_u^{(a+1)}P_u^{(b)} \geq 0,$$

which implies $h_u(a) \geq h_u(b)$. Hence, $h_u(a)$ is decreasing in a. □

Remark 2. *It is easy to see if $a \neq b$, then $h_u(a) = h_u(b)$ if and only if*

$$w_{ux} = w_{uy}$$

for any vertices $x,\ y \sim u$.

Proof of Proposition 1. When $a > -1$, applying Lemma 4, we have $h_u(a) \leq h_u(-1)$, which is equivalent to

$$\frac{P_u^{(a+1)}P_u^{(-1)}}{P_u} \geq P_u^{(0)} = d_u.$$

Combine this with (14), we deduce

$$\sum_{uv\in E} \kappa_{uv} \leq \sum_{u\in V}(2 - d_u) = 2.$$

For the case of $a \leq -1$, the estimates for the sum of curvatures are almost the same and we omit their proofs here.

To see the uniform bounds for κ_{uv}, we have already seen it is no more than two. For the lower bound, notice

$$\kappa_{uv} = \sum_{e\in E} \kappa_e - \sum_{e\in E\setminus\{uv\}} \kappa_e \geq 2 - 2\big(|E| - 1\big) = -2\big(|V| - 3\big),$$

which completes the proof. □

Remark 3. *In the case of $a \neq -1$, if the equality $\sum_{uv\in E} \kappa_{uv} = 2$ holds, then*

$$h_a(u) = h_{-1}(u)$$

holds for any vertex $u \in V$. As mentioned in Remark 2, it then follows

$$w_{ux} = w_{uy}$$

for all vertices $x,\ y$ incident to u. Using the connectivity of the tree, we can deduce that all edges of the tree must be equal.

3.3. **Examples of Ricci Flow Convergence on Trees.** In the following, we present examples of trees exhibiting explicit Ricci flow behavior under the general Ollivier-Ricci curvature (10), focusing on path and star structures.

Example 2. *Consider the Ricci flow (8) with $a \neq -1$ on the path graph of length n, with edges denoted as $e_1, \ldots, e_n$. Then, the Ricci flow converges, and the unnormalized weights on all edges decrease to zero.*

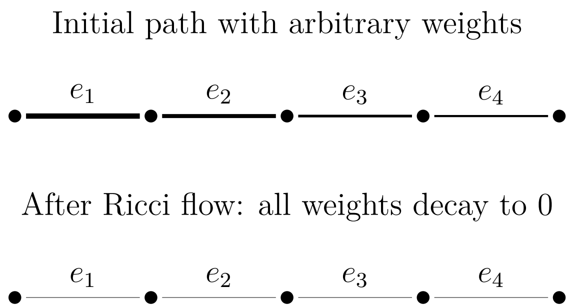

FIGURE 3. Path graph of 5 vertices with edges $e_1, \dots, e_4$. Top: initial edge weights (arbitrary). Bottom: after Ricci flow, all edge weights decay to zero.

sketch of proof. Let w represent the unnormalized weight. By formula (12), we have

$$\begin{aligned}\frac{\partial}{\partial t}\sum_{uv\in E} w_{uv} = -\sum_{uv\in E}\kappa_{uv}w_{uv} &= -\sum_{u\in V}(2-d_u)\frac{\sum_{x\sim u} w_{ux}^{1+a}}{\sum_{x\sim u} w_{xu}^{a}}\\ &= -(w_{e_1}+w_{e_n})\\ &< 0,\end{aligned}$$

for all $t \in [0,\infty)$, so the sum $\sum_{uv\in E} w_{uv}$ of unnormalized weights on all edges decreases in particular, it is bounded and has a non-nonnegative limits. Moreover, weight w_{e_i} of each edge is also bounded. It is easy to check that $w_{e_1}+w_{e_n} \to 0$ and hence $w_1, w_n \to 0$. Now consider

$$\frac{d}{dt}w_{e_1}(t) = -w_{e_1} - \frac{w_{e_1}^{a+1} - w_{e_2}^{a+1}}{w_{e_1}^{a} + w_{e_2}^{a}},$$

which tends to 0 as $w_{e_1} \to 0$. Thus,

$$\frac{w_{e_1}^{a+1} - w_{e_2}^{a+1}}{w_{e_1}^{a} + w_{e_2}^{a}} \to 0,$$

which give $w_2 \to 0$.

By iterating this argument along the chain of edges, we conclude $w_{e_i}(t) \to 0$ for all i.

□

Example 3 (Star Tree)**.** *Consider the Ricci flow* (8) *with $a \geq 0$ on the star tree $K_{1,n}$, $n \geq 4$, with center vertex u and leaf edges $w_i := w_{uv_i}$. The unnormalized on all edges decrease to* 0 *and the normalized weights on all edges converge to $\frac{1}{n}$.*

Initial star graph

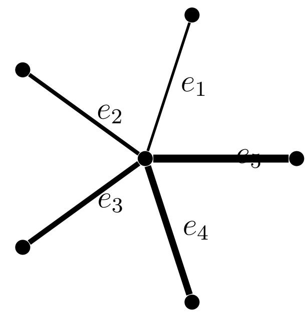

After Ricci flow: edges decay

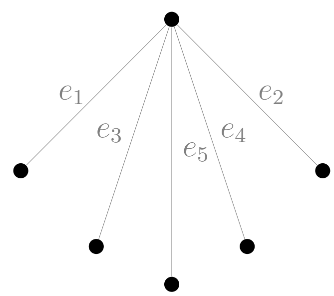

Proof. Let w represent the unnormalized weight. Denote the center vertex as u, using formula (12), we have

$$\frac{\partial \sum\limits_{uv\in E} w_{uv}}{\partial t} = -\sum_{uv\in E} \kappa_{uv} w_{uv} = -\sum_{u\in V} (2-d_u)\frac{\sum_{x\sim u} w_{ux}^{1+a}(t)}{\sum_{x\sim u} w_{ux}^{a}(t)}$$

$$= -\sum_{i=1}^{n} w_i + (n-2)\frac{\sum\limits_{i=1}^{n} w_i^{1+a}}{\sum_{x\sim u} w_i^a}.$$

By the following lemma 5, the leaf weights satisfy $w_i(t)/w_j(t) \to 1$ as $t\to\infty$ for all pairs i,j, and the ratios remain bounded away from 0 and ∞ for all $t>0$. In particular, the normalized weight

$$\tilde{w}_i(t) = \frac{w_i(t)}{\sum_i w_i(t)} \longrightarrow \frac{1}{n}.$$

Moreover, for large $t>0$, we have

$$-\sum_{i=1}^{n} w_i + (n-2)\frac{\sum_{i=1}^{n} w_i^{1+a}}{\sum_{i=1}^{n} w_i^a} \sim -n\sum_{i=1}^{n} w_i + (n-2)\sum_{i=1}^{n} w_i = -2\sum_{i=1}^{n} w_i < 0.$$

Therefore, the sum $\sum_i w_i$ of the unnormalized weights decays to zero exponentially. $\square$

Lemma 5. *Let $a \geq 0$ and let $K_{1,n}$ be the star with center u and leaves $v_1, \ldots, v_n$, $n \geq 4$. Write $w_i(t) := w_{uv_i}(t) > 0$, then for any i and j, we have*

$$\lim_{t \to +\infty} \frac{w_i(t)}{w_j(t)} = 1 \tag{15}$$

Proof. Assume that, at time $t = 0$, we have:

$$w_1(0) \geq w_2(0) \geq \cdots \geq w_n(0).$$

For any $1 \leq i < j \leq n$, we have:

$$\begin{aligned} \frac{\partial}{\partial t} \frac{w_i}{w_j} &= \frac{w_i}{w_j}(\kappa_j - \kappa_i) = \frac{w_i}{w_j} \left(-\frac{\sum_{k=1}^n w_k^{a+1} - 2w_j^{a+1}}{w_j \cdot \sum_{k=1}^n w_k^a} + \frac{\sum_{k=1}^n w_k^{a+1} - 2w_i^{a+1}}{w_i \cdot \sum_{k=1}^n w_k^a} \right) \\ &= (1 - \frac{w_i}{w_j}) \cdot \frac{\sum_{k=1}^n w_k^{a+1} + 2w_i w_j \cdot \frac{w_i^a - w_j^a}{w_i - w_j}}{w_j \cdot \sum_{k=1}^n w_k^a} \end{aligned} \tag{16}$$

Since $w_i/w_j \geq 1$ at $t = 0$, then it holds true for all $t > 0$. In particular, according to (16), w_i/w_j is decreasing and its limit must exist and be finite:

$$\lambda_{ij} := \lim_{t \to \infty} w_i/w_j \in [1,\ w_i(0)/w_j(0)]$$

Thus we have established the (finite) convergence of w_i/w_j for $i < j$. It then follows, for any i and j, the limit of w_i/w_j exists and is a positive real number which will be denoted by λ_{ij}.

Using $a \geq 0$ and $\frac{w_i^a - w_j^a}{w_i - w_j} > 0$, we can deduce the limit

$$\begin{aligned} \lim_{t \to \infty} \frac{\sum_{k=1}^n w_k^{a+1} + 2w_i w_j \cdot \frac{w_i^a - w_j^a}{w_i - w_j}}{w_j \cdot \sum_{k=1}^n w_k^a} &\geq \lim_{t \to \infty} \frac{\sum_{k=1}^n w_k^{a+1}}{w_j \cdot \sum_{k=1}^n w_k^a} = \lim_{t \to \infty} \frac{\sum_{k=1}^n (w_k/w_j)^{a+1}}{\sum_{k=1}^n (w_k/w_j)^a} \\ &= \frac{\sum_{k=1}^n \lambda_{kj}^{a+1}}{\sum_{k=1}^n \lambda_{kj}^a} \end{aligned}$$

must be bounded below by a positive number. In particular, there exists some positive constant $C > 0$ such that:

$$\frac{\sum_{k=1}^n w_k^{a+1} + 2w_i w_j \frac{w_i^a - w_j^a}{w_i - w_j}}{w_j \cdot \sum_{k=1}^n w_k^a} \geq C. \tag{17}$$

Combine (17) with (16), in case of $i < j$ where $w_i \geq w_j$, we obtain

$$\frac{\partial}{\partial t} \frac{w_i}{w_j} \leq C(1 - \frac{w_i}{w_j}).$$

Therefore

$$0 \leq \frac{w_i(t)}{w_j(t)} - 1 \leq \left(\frac{w_i(0)}{w_j(0)} - 1 \right) \exp(-Ct)$$

for $t > 0$ and (15) follows. □

3.4. **Uniform Lower Bounds on Normalized Weights on Internal Edges for $a > -1$.**

Proposition 5. *Consider the Ricci flow* (8) *with $a \geq -1$ on any tree. Then the normalized weights on internal edges admit a uniform positive lower bound.*

Proof. Let $w(t) = \min_{e \in E} w_e(t)$. We will show that $w(t)$ never decreases to zero on internal edges. Assume at time t, $w_{xy}(t) = w(t)$, because $a+1 > 0$ each term $w_{xz}^{a+1} \geq w^{a+1}$ by the minimality of w. Hence

$$\sum_{z\sim x,\, z\neq y} w_{xz}^{a+1} \geq (d_x - 1)w^{a+1}.$$

Rewrite the x-contribution of κ_{xy} as

$$\frac{w^a}{P_x^{(a)}} - \frac{1}{w} \cdot \frac{\sum_{z\sim x,\, z\neq y} w_{xz}^{a+1}}{P_x^{(a)}} = \frac{w^{a+1} - \sum_{z\sim x,\, z\neq y} w_{xz}^{a+1}}{wP_x^{(a)}}.$$

Using the lower bound for the sum,

$$w^{a+1} - \sum_{z\sim x,\, z\neq y} w_{xz}^{a+1} \leq w^{a+1} - (d_x - 1)w^{a+1} = (2 - d_x)w^{a+1}.$$

Therefore

$$\frac{w^{a+1} - \sum_{z\sim x,\, z\neq y} w_{xz}^{a+1}}{wP_x^{(a)}} \leq \frac{(2 - d_x)w^{a+1}}{wP_x^{(a)}} = (2 - d_x)\,\frac{w^a}{P_x^{(a)}}.$$

Similarly, result for the y-contribution of κ_{xy}.

Thus, if xy is an internal edge, then both $d_x \geq 2, d_y \geq 2$, we have $\kappa_{xy}(t) \leq 0$, then $\frac{\partial w_{xy}}{\partial t} \geq 0$, resulting that w_{xy} does not decrease at time t. Therefore, there is a uniform bound on the normalized weight of all internal edges.

□

4. The Ricci flow with parameter $a = 0$

We prove the convergence of the Ricci flow on trees in the case $a = 0$. In this case, the Lin-Lu-Yau Ricci curvature on tree is expressed as

$$\kappa_{xy} = -\frac{\sum_{z\sim x} w_{xz}}{w_{xy}d_x} + \frac{2}{d_x} + \frac{2}{d_y} - \frac{\sum_{z\sim y} w_{yz}}{w_{xy}d_y}.$$

4.1. **The Ricci Flow Equations.**

4.1.1. *The Unormalized Ricci Flow.* The unormalized Ricci flow is

$$\frac{\partial}{\partial t} w_{xy}(t) = -\left(\frac{1}{d_x} + \frac{1}{d_y}\right) w_{xy}(t) + \frac{1}{d_x} \sum_{u\sim x,\ u\neq y} w_{xu}(t) + \frac{1}{d_y} \sum_{v\sim y,\ v\neq x} w_{vy}(t). \tag{18}$$

This system of differential equations is linear with the coefficient matrix R:

$$R_{e,e'} = \begin{cases} -(\frac{1}{d_x} + \frac{1}{d_y}) & \text{if } e = e' = \{x, y\}, \\ \frac{1}{d_x} & \text{if } e \cap e' = \{x\}, \\ 0 & \text{if } e \cap e' = \emptyset, \end{cases} \tag{19}$$

which will be called the **Ricci flow evolution matrix**.

4.1.2. *The Normalized Ricci Flow.* Since

$$\sum_{xy\in E} \kappa_{xy}\cdot w_{xy} = 2\sum_{xy\in E}\left(\frac{1}{d_x}+\frac{1}{d_y}-1\right)w_{xy},$$

then we obtain the normalized continuous Ricci flow in the case of $a=0$:

$$\begin{aligned}\frac{\partial w_{xy}(t)}{\partial t} &= 2\sum_{uv\in E}\left(\frac{1}{d_u}+\frac{1}{d_v}-1\right)w_{uv}(t)\cdot w_{xy}(t)\\ &\quad -\left(\frac{1}{d_x}+\frac{1}{d_y}\right)w_{xy}(t)+\frac{1}{d_x}\sum_{u\sim x,\ u\neq y} w_{xu}(t)+\frac{1}{d_y}\sum_{v\sim y,\ v\neq x} w_{vy}(t).\end{aligned} \tag{20}$$

4.2. **The Einstein Metrics.** It is natural to consider the static solution

$$w(\infty)=\{w_e(\infty)\}_{e\in E}\in\mathbb{R}_+^E$$

of the normalized Ricci flow.

Definition 3. *If a normalized metric $w=(w_e)_{e\in E}\in\mathbb{R}_+^E$ satisfies:*

$$\kappa_e(\infty)=\kappa \tag{21}$$

*for all $e\in E$ where $\kappa\in\mathbb{R}$ is some constant, then the metric/weight function is called the **metric of constant curvature** or **Einstein metric**.*

In the case of $a=0$, we see a metric $w=(w_e)_{e\in E}\in\mathbb{R}_+^E$ has constant curvatue κ if and only if

$$\left(\frac{1}{d_x}+\frac{1}{d_y}-\kappa\right)w_{xy}=\frac{1}{d_x}\sum_{u\sim x,\ u\neq y} w_{xu}(t)+\frac{1}{d_y}\sum_{v\sim y,\ v\neq x} w_{vy}(t). \tag{22}$$

for any edges $e=xy\in E$. Rearranging the terms in equation (22) gives

$$-\left(\frac{1}{d_x}+\frac{1}{d_y}\right)w_{xy}+\frac{1}{d_x}\sum_{u\sim x,\ u\neq y} w_{xu}+\frac{1}{d_y}\sum_{v\sim y,\ v\neq x} w_{vy}=-\kappa\, w_{xy}.$$

The left-hand side is precisely the e-th component of Rw as defined in (19). Hence,

$$(Rw)_e=-\kappa\, w_e,\quad \forall\, e\in E,$$

which means that w is an eigenvector of the evolution matrix R with eigenvalue $-\kappa$.

In the next subsection, we shall prove the existence of an Einstein metric on a tree for the case $a=0$ using the Ricci flow. Before turning to existence, we first establish a uniqueness result.

Recall from (19) that we introduced the matrix R, originally as the coefficient matrix of the unnormalized Ricci flow. However, it is important to note that R is defined purely in terms of the combinatorial structure of the tree. In particular, equation (22) shows that an Einstein metric w satisfies $Rw=-\kappa w$, so Einstein metrics correspond exactly to eigenvectors of R. This observation allows us to prove the uniqueness without referring to the flow itself.

Proposition 6 (Uniqueness of Einstein Metric)**.** *Let $T = (V, E)$ be a tree. Suppose $w, w^* \in \mathbb{R}_+^E$ are two (normalized) metrics on T of constant curvatures κ and κ^*, respectively. Then $w = w^*$ and $\kappa = \kappa^*$.*

Proof. Notice that if $\kappa \neq \kappa^*$, then w and w^*, as corresponding eigenvectors of the symmetric matrix R (see (19)), must be orthogonal. This is equivalent to:

$$\sum_{e \in E} w_e \cdot w_e^* = 0.$$

which contradicts with $w_e > 0$ and $w_e^* > 0$. Therefore $\kappa = \kappa^*$. Now we set

$$r = \min\{w_e \cdot (w_e^*)^{-1} : \ e \in E\} > 0,$$

it then follows $\hat{w} := w - r \cdot w^*$ defines a nonnegative weight function satisfying (22) with $\hat{w}_{xy} = 0$ for some edge $e_0 = xy$. According to (22), we have:

$$0 = \left(\frac{1}{d_x} + \frac{1}{d_y} - \kappa\right)\hat{w}_{xy} = \frac{1}{d_x}\sum_{u \sim x,\ u \neq y} \hat{w}_{xu}(t) + \frac{1}{d_y}\sum_{v \sim y,\ v \neq x} \hat{w}_{vy}(t).$$

Therefore $\hat{w}_e = 0$ for all $e \in N(x) \cup N(y)$. Repeating this process and using the connectivity of the tree, we can show $\hat{w}_e = 0$ for all edges and $w = r \cdot w^*$. Since both of them are normalized metrics, then we have $r = 1$ and $w = w^*$.

□

4.3. **Convergence of the Normalized Ricci Flow.** The main result was stated in the Introduction. For clarity, we present it again below.

Theorem 2 (Convergence of Ricci Flow on Weighted Trees)**.** *Let $T = (V, E, w_0)$ be a finite, weighted tree with edge weights being strictly positive. Let $w = w(t)$ be the Ricci flow (18) on T with initial weight w_0.*

*(1) **(Long time existence)** The solution $w = w(t)$ exists uniquely for any positive initial metric and for all time $t > 0$. Under the flow, $w_e(t) > 0$ for all $t > 0$ and $e \in E$.*
*(2) **(Convergence to equilibrium)** The normalized Ricci flow (20) converges to an Einstein metric $w(\infty)$ with curvature $\kappa(\infty)$. In particular, a tree $T = (V, E)$ always admits a unique Einstein metric in sense of (21) in the case of $a = 0$.*
*(3) **(Limit behavior)** The limit curvature $\kappa(\infty)$ equals to minus of the largest eigenvalue of the evolution matrix of the Ricci flow.*

Proof of part (1). Let $w(t) = (w_e(t))_{e \in E}$ denote the vector of edge weights at time t, with initial data $w(0) > 0$. Since the Ricci flow define a system of linear ordinary equations:

$$\frac{\partial}{\partial t} w(t) = R w(t) \tag{23}$$

where R is the evolution matrix of the Ricci flow (19), then the solution is unique and can be written as:

$$w(t) = \exp(R \cdot t) w(0) \tag{24}$$

for all $t \geq 0$. Moreover, according to the Proof of Theorem 3 in [2], $w_e(t) > 0$ for every edge e and all the time since $w_e(0) > 0$. Those complete the proof of (1). □

Proof of part (2). Let $\lambda_1 < \lambda_2 < \cdots < \lambda_s$ be all the distinct eigenvalues of the evolution matrix R. As a real symmetric matrix, R must be diagonalizable. Therefore, using (24), the general solution $w = w(t)$ of the flow has following form:

$$w_e(t) = \sum_{i=1}^{s} c_{i,e} \exp(\lambda_i t). \tag{25}$$

where $c_{i,e}, 1 \leq i \leq s, \ e \in E$ represent some real constants.

It is clear that the coefficients $c_{i,e}$ in (25) can not be all zeros. Thus we can define the index i_0 to be the largest one with $c_{i,e} \neq 0$ for some $e \in E$:

$$i_0 := \max \left\{1 \leq i \leq s : \exists\, e_0 \in E \text{ such that } c_{i,e_0} \neq 0\right\}. \tag{26}$$

Claim 1. *$c_{i_0,e} > 0$ for all $e \in E$.*

Proof of the Claim. For any edge $e \in E$, according to part (1), $w_e(t) > 0$ for all $t > 0$. Thus we have:

$$c_{i_0,e} = \lim_{t\to\infty} \frac{w_e(t)}{\exp(\lambda_{i_0} t)} \geq 0.$$

Now suppose $c_{i_0,e} = 0$ for some edge $e = xy$. Comparing the coefficients of $\exp(\lambda_{i_0} t)$ on both sides of (18), we have:

$$\left(\frac{1}{d_x} + \frac{1}{d_y} - \lambda_{i_0}\right) c_{i_0,xy} = \frac{1}{d_x} \sum_{u\sim x,\ u\neq y} c_{i_0,xu} + \frac{1}{d_y} \sum_{v\sim y,\ v\neq x} c_{i_0,yv}. \tag{27}$$

Noting that $c_{i_0,xy} = 0$, we deduce:

$$0 = \frac{1}{d_x} \sum_{u\sim x,\ u\neq y} c_{i_0,xu} + \frac{1}{d_y} \sum_{v\sim y,\ v\neq x} c_{i_0,yv}.$$

Thus the non-negativity of $c_{i_0,e'}$ yields $c_{i_0,e'} = 0$ for all edges $e' \in N(x) \cup N(y)$. Repeating this process to the new edges e' with $c_{i_0,e'} = 0$ and using the connectivity of the graph, we conclude $c_{i_0,e} = 0$ for all edgs e which contradicts with (26). Therefore, $c_{i_0,e}$ must be positive for every edge e. □

By the above claim 1, we can rewrite

$$w_e(t) = \sum_{i=1}^{i_0} c_{i,e} \exp(\lambda_i t). \tag{28}$$

with $c_{i_0,e} > 0$ for all edges e. It then follows that the normalized weight $\tilde{w}_e(t)$ must converge and:

$$\begin{aligned}\lim_{t\to\infty} \tilde{w}_e(t) &= \lim_{t\to\infty} \frac{w_e(t)}{\sum_{e'\in E} w_{e'}(t)} \\ &= \lim_{t\to\infty} \frac{c_{i_0,e}\exp(\lambda_{i_0}t) + o(\exp(\lambda_{i_0}t))}{\sum_{e'\in E} c_{i_0,e'}\exp(\lambda_{i_0}t) + o(\exp(\lambda_{i_0}t))} \\ &= \frac{c_{i_0,e}}{\sum_{e'\in E} c_{i_0,e'}},\end{aligned} \tag{29}$$

which is positive and will be denoted as $\tilde{w}_e(\infty)$. Notice that (27) implies $\tilde{w} = (\tilde{w}_e(\infty))_{e\in E}$ is an Einstein metric with curvature $-\lambda_{i_0}$ in sense of (22). Thus we have proved that the limit metric exists and must be an Einstein metric.

Moreover, using the flow equation (23) and (28), we can compute the limit of the Ricci curvatures:

$$\begin{aligned}\lim_{t\to\infty} \kappa_e(t) &= -\lim_{t\to\infty} \frac{1}{w_e(t)} \frac{\partial}{\partial t} w_e(t) = -\lim_{t\to\infty} \frac{\lambda_{i_0} c_{i_0,e}\exp(\lambda_{i_0}t)}{c_{i_0,e}\exp(\lambda_{i_0}t)} \\ &= -\lambda_{i_0},\end{aligned} \tag{30}$$

This proves the convergence and finishes the proof of part (2).

□

Proof of part (3). Note that the Einstein metric $w = (w_e)^T_{e\in E}$ is an eigenvector of R corresponding to eigenvalue $-\kappa$ (see section 4.2). In the following, we shall show such eigenvalue is the largest one.

Let μ be any eigenvalue of R with a (nonzero) eigenvector $v = (v_e)_{e\in E} \in \mathbb{R}^E$.

Note that the entries of $2I + R$ are non-negative, then we have:

$$(2+\mu)|v_e| = \left|\sum_{e'\in E}(2\delta_{e,e'} + R_{e,e'})v_{e'}\right| \le \sum_{j=1}^{m}(2\delta_{e,e'} + R_{e,e'})|v_e|,$$

where $\delta_{e,e'}$ equals one if $e = e'$ and zero otherwise. As the entries of $w = (w_e)^T_{e\in E}$ are positive, it then follows:

$$\begin{aligned}\sum_{e\in E}(2+\mu)w_e|v_e| &\le \sum_{e\in E}^{m}\sum_{e'\in E} w_e(2\delta_{e,e'} + R_{e,e'})|v_{e'}| \\ &= \sum_{e'\in E}\Big(\sum_{e\in E} w_e(2\delta_{e,e'} + R_{e,e'})\Big)|v_{e'}| = \sum_{e'\in E}(2-\kappa)w_{e'}|v_{e'}|\end{aligned} \tag{31}$$

which yields:

$$(\mu+\kappa)\sum_{e\in E} w_e|v_e| \le 0.$$

Therefore, we conclude $\mu \le -\kappa$ which completes the proof. □

4.4. **Bounds for the Limit Curvature.** In the last subsection, we have seen that the Ricci flow is always convergent to the unique Einstein metric. It is natural to classify graphs/trees according to the curvature of the unique Einstein metrics that they can support. Because in classical differential geometry (eg. the uniformization theorem in dimension two), the curvatures of Einstein metric give strong restriction on the geometry and topology of the underlying manifolds. In this subsection, we mainly study those curvatures of a tree and derive some bounds for them.

Proposition 7. *Let κ be the curvature of the Einstein metric. Then:*

$$2\min_{xy\in E}\left(\frac{1}{d_x}+\frac{1}{d_y}-1\right)\le\kappa\le\frac{2}{|E|}, \tag{32}$$

Any one of the equalities holds if and only if G is a star graph.

Proof. Let $\{w_e\}_{e\in E}$ be the normalized weight of the Einstein metric. Assume $e_0 = xy$ is the edge with the largest weight, then by (22)

$$\begin{aligned}
\kappa\cdot w_{e_0} &= \left(\frac{1}{d_x}+\frac{1}{d_y}\right)w_{e_0}-\frac{1}{d_x}\sum_{e'\in N(x)\setminus e_0}w_{e'}-\frac{1}{d_y}\sum_{e''\in N(x)\setminus e_0}w_{e''}\\
&\ge\left(\frac{1}{d_x}+\frac{1}{d_y}\right)w_{e_0}-\frac{1}{d_x}\sum_{e'\in N(x)\setminus e_0}w_{e_0}-\frac{1}{d_y}\sum_{e''\in N(x)\setminus e_0}w_{e_0}\\
&=2\left(\frac{1}{d_x}+\frac{1}{d_y}-1\right)w_{e_0}\\
&\ge 2\min_{xy\in E}\left(\frac{1}{d_x}+\frac{1}{d_y}-1\right)w_{e_0}.
\end{aligned} \tag{33}$$

Since $w_{e_0}>0$, dividing through by w_{e_0} yields the lower bound for κ. For the upper bound, recall in Proposition 1, we have shown that $\sum_{e\in E}\kappa_e\le 2$. Therefore in the case of an Einstein metric where $\kappa_e=\kappa$ for any $e\in E$, we obtain the upper bound:

$$\kappa\le\frac{2}{|E|}$$

In the next, we shall consider the case when one of two equalities holds. We claim: in both cases, all the weights w_e take the same value and as a corollary,

$$\kappa=\frac{2}{d_x}+\frac{2}{d_y}-2 \tag{34}$$

for any $xy\in E$.

(1) Suppose κ attains the lower bound in (32):

$$\kappa=\min\left\{\frac{2}{d'_x}+\frac{2}{d'_y}-2:\ x'y'\in E\right\}.$$

Once again, let $e_0 = xy$ be the edge with largest weight w_{e_0}. It then follows from (33), equality holds only if $w_{e'}=w_{e_0}$ for all $e'\in N(x)\cup N(y)$, and

$$\kappa=2\left(\frac{1}{d_x}+\frac{1}{d_y}-1\right)$$

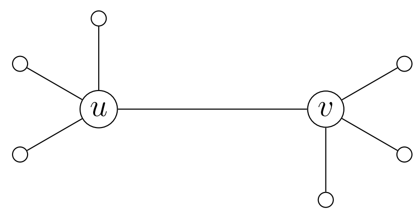

Since T is connected, repeating this process, we will get $w_e = w_{e_0}$ for all $e \in E$.

(2) Suppose κ attains the upper bound in (32):

$$\kappa = \frac{2}{|E|},$$

then we have $\sum_{uv \in E} \kappa_{uv} = 2$. According to the discussion in Remark 3, we see all the weights w_e must be equal.

Now we consider the graph G with properties (34). Let x be a vertex with maximum degree d. We claim every edge incident to x is a leaf edge. Otherwise, let $e = xy$ be an internal edge and $e' = x'y'$ a leaf edge. Then:

$$\frac{1}{d_{x'}} + \frac{1}{d_{y'}} \;\geq\; 1 + \frac{1}{d} \;>\; \frac{1}{2} + \frac{1}{d} \;\geq\; \frac{1}{d_x} + \frac{1}{d_y},$$

which contradicts with (34). Thus, G must be a star. Conversely, if G is a star with center degree d, then $\kappa = \frac{2}{d}$ which achieves both upper and lower bounds in (32). ☐

Remark 4. *For non-star tree, that is, trees that contain internal edges, we have a more explicit bound,*

$$2 \min_{\substack{xy \in E \\ xy \text{ internal}}} \left(\frac{1}{d_x} + \frac{1}{d_y} - 1 \right) \;<\; \kappa \;<\; \frac{2}{|E|}$$

4.5. **Examples of Double Star Trees.** We now show some trees whose curvatures of their Einstein metrics are positive, zero or negative.

Example 4 ("double-star" trees)**.** *We consider a graph with only one internal edge $e = \{u, v\}$. Assume the degree of u and v are $n+1$. In this graph, let $-\kappa$ be the maximum eigenvalue of R and the entries of the corresponding eigenvector are $z, x_1 \cdots, x_n, y_1, \cdots, y_n$. Therefore we have:*

$$\kappa \cdot z = \frac{2}{n+1} z - \frac{1}{n+1} \sum_{i=1}^{n} x_i - \frac{1}{n+1} \sum_{i=1}^{n} y_i \tag{35}$$

$$\kappa \cdot x_j = \frac{n+2}{n+1} x_j - \frac{1}{n+1} \sum_{i \neq j} x_i - \frac{1}{n+1} z, \quad i = 1, 2, \cdots, n \tag{36}$$

$$\kappa \cdot y_j = \frac{n+2}{n+1} y_j - \frac{1}{n+1} \sum_{i \neq j} y_i - \frac{1}{n+1} z, \quad j = 1, 2, \cdots, n \tag{37}$$

From (36) and (37), we add them up to deduce:

$$\left(\frac{3}{n+1}-\kappa\right)\sum_{i=1}^{n} x_i = \frac{n}{n+1}z, \quad \left(\frac{3}{n+1}-\kappa\right)\sum_{i=1}^{n} y_i = \frac{n}{n+1}z, \tag{38}$$

Combine (35) and (38) together, we get:

$$\left(\frac{2}{n+1}-\kappa\right)\left(\frac{3}{n+1}-\kappa\right) = \frac{2n}{(n+1)^2}$$

which is equivalent to:

$$\kappa^2 - \frac{5}{n+1}\kappa + \frac{6-2n}{(n+1)^2} = 0 \tag{39}$$

Applying Theorem 1, we can conclude the behavior of the Ricci flow: when $n < 3$, $\kappa > 0$, *the unnormalized weights of all edges decay to zero; when* $n = 3$, $\kappa = 0$, *the unnormalized weights of all edges converge to some positive numbers; when* $n > 3$, $\kappa < 0$, *the unnormalized weights of all edges grow without bound.*

This theoretical result is illustrated by the numerical simulations in Figure 4, where we plot the weight evolution for the double-star trees with $n = 2, 3, 4$.

4.6. **Alternating Sum of the Curvatures Along Path.** The constant-curvature metrics play a key role in understanding the limiting behavior of the Ricci flow on trees. We derive an identity relating the curvature values and the edge weights of an Einstein metric along a path connecting two leaves.

Proposition 8 (Alternating Sum Identity on Path of all Trees)**.** *Let* $T = (V, E, w)$ *be a finite weighted tree with positive edge weights* $w : E \to \mathbb{R}_{>0}$. *Assume* w *is a metric of constant curvature.*

Let $P = (v_0, v_1, \ldots, v_k)$ *be a path in the tree, with corresponding edges* $e_i = v_{i-1}v_i$ *for* $i = 1, \ldots, k$ *where* v_0 *and* v_k *are leaf nodes, then we have*

$$\sum_{i=1}^{k}(-1)^{i-1}\kappa\cdot w_{e_i} = -w_{e_1} + (-1)^k w_{e_k} + \sum_{i=1}^{k}(-1)^{i-1}\left(\frac{2}{d_{v_{i-1}}}+\frac{2}{d_{v_i}}\right)w_{e_i}. \tag{40}$$

Proof. Since κ is constant, using the notation $P_x := \sum_{y\sim x} w_{xy}$, we may write:

$$\kappa\cdot w_{e_i} = -\frac{P_{v_{i-1}}}{d_{v_{i-1}}} + \frac{2w_{e_i}}{d_{v_{i-1}}} + \frac{2w_{e_i}}{d_{v_i}} - \frac{P_{v_i}}{d_{v_i}}.$$

Take the alternating sum over the path:

$$\sum_{i=1}^{k}(-1)^{i-1}\kappa\cdot w_{e_i} = \sum_{i=1}^{k}(-1)^{i-1}\left(-\frac{P_{v_{i-1}}}{d_{v_{i-1}}} + \frac{2w_{e_i}}{d_{v_{i-1}}} + \frac{2w_{e_i}}{d_{v_i}} - \frac{P_{v_i}}{d_{v_i}}\right).$$

Split the sum:

$$\sum_{i=1}^{k}(-1)^{i-1}\kappa w_{e_i} = \sum_{i=1}^{k}(-1)^{i}\frac{P_{v_{i-1}}}{d_{v_{i-1}}} - \sum_{i=1}^{k}(-1)^{i+1}\frac{P_{v_i}}{d_{v_i}}$$

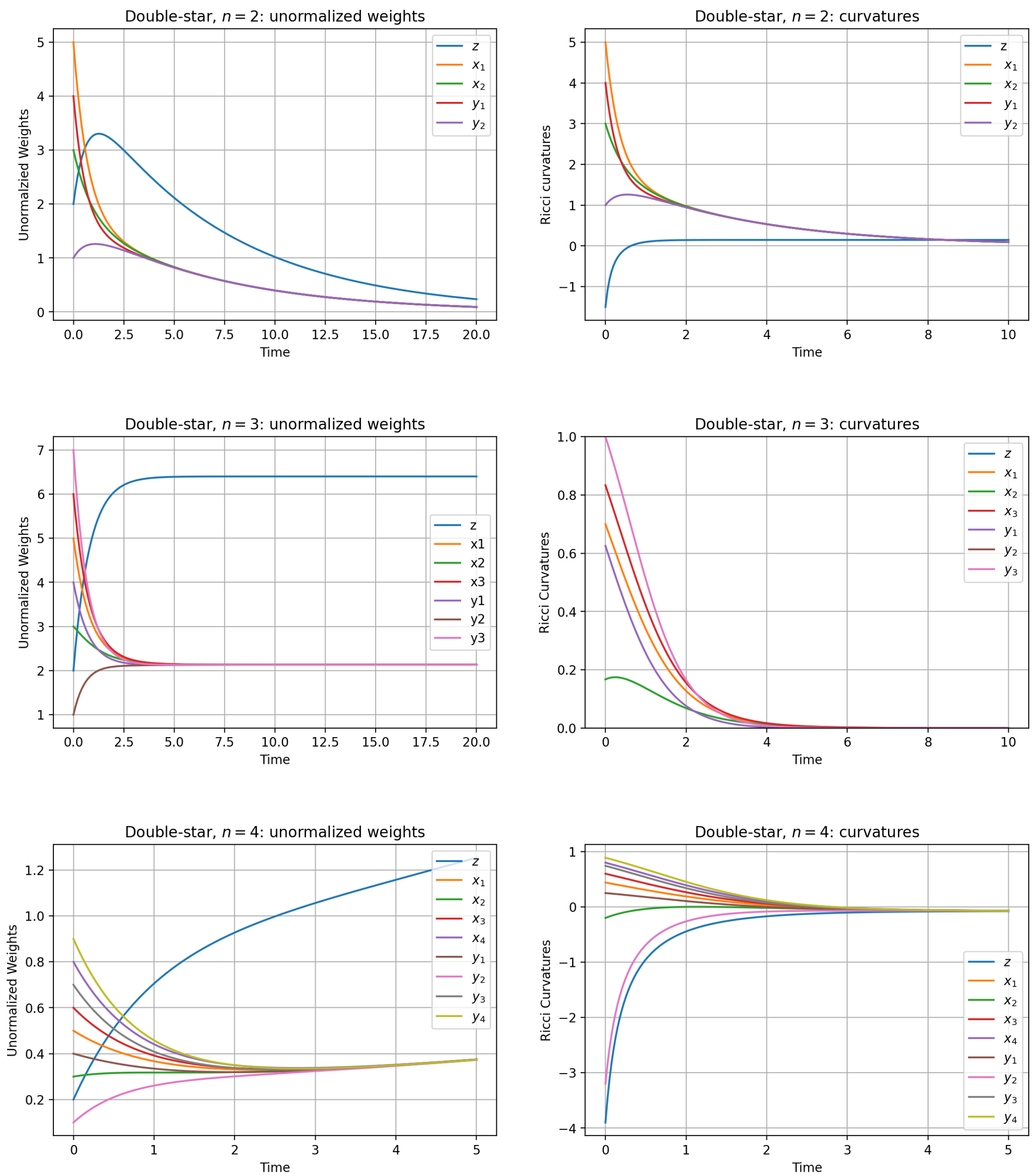

FIGURE 4. Unnormalized Ricci Flow on Double-Stars with $n = 2,\ 3,\ 4$.

$$+\sum_{i=1}^{k}(-1)^{i-1}\left(\frac{2}{d_{v_{i-1}}}+\frac{2}{d_{v_i}}\right)w_{e_i}.$$

Observe that the sum over P_{v_i} telescopes:

$$\sum_{i=1}^{k}(-1)^{i}\frac{P_{v_{i-1}}}{d_{v_{i-1}}}-\sum_{i=1}^{k}(-1)^{i+1}\frac{P_{v_i}}{d_{v_i}}=-\frac{P_{v_0}}{d_{v_0}}+(-1)^{k}\frac{P_{v_k}}{d_{v_k}}.$$

Thus, we conclude:

$$\sum_{i=1}^{k}(-1)^{i-1}\kappa w_{e_i} = -\frac{P_{v_0}}{d_{v_0}} + (-1)^k\frac{P_{v_k}}{d_{v_k}} + \sum_{i=1}^{k}(-1)^{i-1}\left(\frac{2}{d_{v_{i-1}}} + \frac{2}{d_{v_i}}\right)w_{e_i}.$$

If v_0 and v_k are leaves, then $d_{v_0} = d_{v_k} = 1$ and $P_{v_0} = w_{e_1}$, $P_{v_k} = w_{e_k}$, giving (40). □

4.7. **More Discussions.** We display more results about the eigenvalues of the Ricci flow matrix and give necessary conditions such that the matrix R has positive eigenvalues.

Observation 1. *Let R be the Ricci flow evolution matrix of a tree T with n vertices. Define*

$$R_e := \sum_{f\neq e}|R_{e,f}|$$

to be the sum of the absolute values of the non-diagonal entries in the e-th row of R.

Then we have the following observations regarding its eigenvalues:

(1) ***Leaf edges:*** *An edge connected to a leaf (degree 1 vertex) contributes negatively to the eigenvalue spectrum. This follows from Gershgorin's circle theorem: for a leaf edge $e = xy$ with $d_x = 1$, the corresponding Gershgorin disk satisfies*

$$R_{e,e} + R_e = -\frac{2}{d_y} < 0.$$

(2) ***Internal edges:*** *For an internal edge $e = xy$, the rightmost point of its Gershgorin disk is*

$$R_{e,e} + R_e = 2 - 2\Big(\frac{1}{d_x} + \frac{1}{d_y}\Big),$$

which may be non-negative if the sum of degrees of its endpoints is at least 5. Equality holds when $d_x = d_y = 2$.

(3) ***Sum of eigenvalues:*** *The sum of all eigenvalues of R equals $-|V|$, since*

$$\sum_i \lambda_i = \mathrm{trace}(R) = -\sum_{xy\in E}\left(\frac{1}{d_x} + \frac{1}{d_y}\right) = -\sum_{x\in V} 1 = -|V|.$$

Additionally, the leftmost point of every Gershgorin disk is -2, so all eigenvalues are greater than -2.

5. Classification of Tree Structures Based on Ricci Flow Spectral Features

The Ricci flow (18) naturally induces an *Evolution Matrix* on trees, capturing edge–edge interactions under curvature evolution. In this section, we illustrate how this matrix can be used to analyze and cluster different tree structures, highlighting the practical utility of the Ricci flow framework. To evaluate its effectiveness, we perform a tree classification task comparing the evolution matrix R with three classical representations: the Adjacency Matrix, the Laplacian Matrix, and the Distance Matrix. Our results indicate that R achieves clearer separation between tree types, emphasizing its superior capability to capture both local and global structural differences relative to standard matrix representations.

We next recall the definitions of the various matrices used in this study:

Definition 4 (Evolution Matrix from Ricci Flow on Trees). *Let $T = (V, E)$ be a finite tree. Index the rows and columns of a matrix $R \in \mathbb{R}^{|E|\times|E|}$ by the edges of T. For an edge $e = \{x, y\} \in E$ and another edge $e' = \{u, v\} \in E$, define*

$$R_{e,e'} = \begin{cases} -\left(\dfrac{1}{d_x} + \dfrac{1}{d_y}\right), & \text{if } e = e', \\ \dfrac{1}{d_x}, & \text{if } e \cap e' = \{x\}, \\ \dfrac{1}{d_y}, & \text{if } e \cap e' = \{y\}, \\ 0, & \text{otherwise}, \end{cases}$$

where d_x and d_y denote the degrees of vertices x and y.

Definition 5 (Adjacency Matrix). *Let $G = (V, E)$ be a simple undirected graph with $V = \{v_1, v_2, \ldots, v_n\}$. The* adjacency matrix *of G is defined as*

$$A = [a_{ij}]_{1\le i,j\le n}, \quad a_{ij} = \begin{cases} 1, & \{v_i, v_j\} \in E, \\ 0, & \text{otherwise.} \end{cases}$$

Definition 6 (Laplacian Matrix). *The* Laplacian matrix *of G is defined by*

$$L = D - A = [\ell_{ij}]_{1\le i,j\le n}, \quad \ell_{ij} = \begin{cases} d_i, & i = j, \\ -1, & i \ne j \text{ and } \{v_i, v_j\} \in E, \\ 0, & \text{otherwise}, \end{cases}$$

where the degree matrix *of G is the diagonal matrix*

$$D = \operatorname{diag}(d_1, d_2, \ldots, d_n).$$

Definition 7 (Distance Matrix). *Let $G = (V, E)$ be a connected simple undirected graph with $V = \{v_1, v_2, \ldots, v_n\}$. The* distance matrix *of G is defined as*

$$D_{dist} = [d(i, j)]_{1\le i,j\le n}, \quad d(i, j) = \begin{cases} 0, & i = j, \\ \text{the length of the shortest path between } v_i \text{ and } v_j, & i \ne j. \end{cases}$$

Experimental Setup The experiments are designed to classify random trees generated by three different models:

- **Prüfer Random (PR) Trees**: Uniformly sampled from the set of all labeled trees with n vertices using random Prüfer sequences.
- **Barabási–Albert (BA) Trees**: Generated by the preferential attachment model with $m = 1$, resulting in a scale-free tree with a heavy-tailed degree distribution.

- **Complete Binary (CB) Trees**: Fully filled at all levels except possibly the last, providing regular hierarchical structures as baselines.

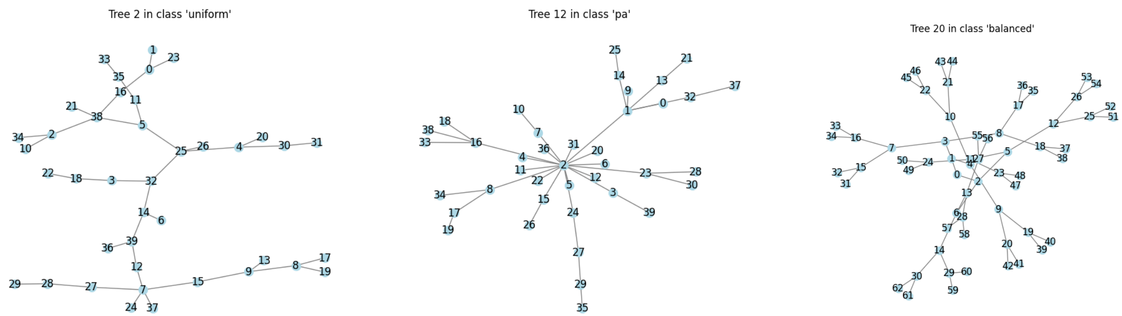

FIGURE 5. Structural examples of Prüfer Random Tree, BA Tree and Complete Binary Tree

These tree models span a range from highly random to highly structured topologies. If the matrices can capture the tree structure differences, it is natural to cluster the trees generated by different tree models basing on the matrices information. Thus, we design a tree classification procedure (as illustrated in Figure: (6) to extract the matrices information and cluster the trees. Code is available at: https://github.com/suyangban/evolution-matrix-based-tree-classification.

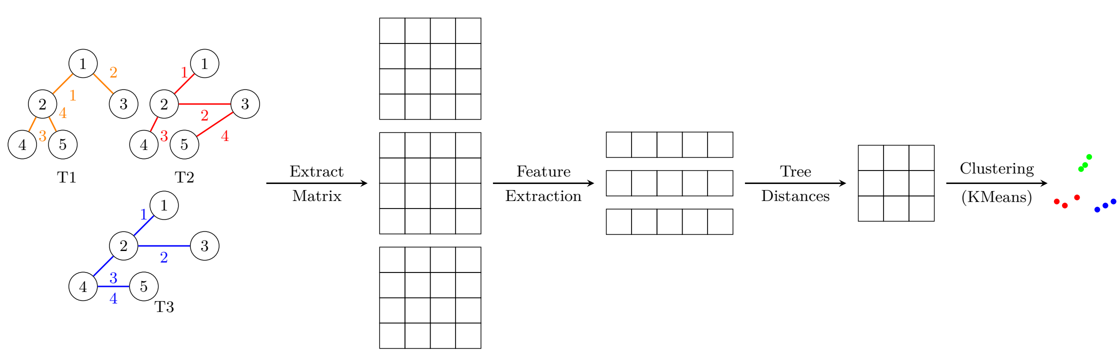

FIGURE 6. A sketch of model process.

Feature Extraction We propose the following steps to extract tree-wise spectral signatures from different matrices:

(1) Compute all eigenvalues and eigenvectors.

(2) Extract statistical descriptors from eigenvalues: Let $\mathbf{x} = [x_1, x_2, \ldots, x_n]^T$ be a vector of real values (e.g., eigenvalues). The statistic variables we used to describe tree spectrum are listed below:

Statistic	Formula
Minimum	$\min(\mathbf{x})$
Median	$\text{median}(\mathbf{x})$
Maximum	$\max(\mathbf{x})$
Mean	$\mu = \frac{1}{n}\sum_{i=1}^{n} x_i$
Std	$\sigma = \sqrt{\frac{1}{n}\sum_{i=1}^{n}(x_i-\mu)^2}$
Variance	$\frac{1}{n}\sum_{i=1}^{n}(x_i-\mu)^2$
Skewness	$\frac{1}{n}\sum_{i=1}^{n}\left(\frac{x_i-\mu}{\sigma}\right)^3$
Kurtosis	$\frac{1}{n}\sum_{i=1}^{n}\left(\frac{x_i-\mu}{\sigma}\right)^4$
Percentile p	$\text{percentile}_p(\mathbf{x})$
Proportion$_{>0}$	$\frac{1}{n}\sum_{i=1}^{n}\mathbb{I}(x_i > 0)$
Proportion$_{=0}$	$\frac{1}{n}\sum_{i=1}^{n}\mathbb{I}(x_i = 0)$
Proportion$_{<0}$	$\frac{1}{n}\sum_{i=1}^{n}\mathbb{I}(x_i < 0)$

(3) From the eigenvector associated with the largest eigenvalue, compute a normalized histogram. Let $\lambda_{\max}$ be the largest eigenvalue, and $\mathbf{v}_{\max} = [v_1, v_2, \ldots, v_n]^T$ the corresponding eigenvector. By Theorem 1, this eigenvector for matrix R is positive, but for other matrix, it can be negative. Thus, we normalize the absolute value of the max eigenvetor by:

$$\mathbf{p} = \left[\frac{|v_1|}{\sum_{j=1}^{n}|v_j|}, \frac{|v_2|}{\sum_{j=1}^{n}|v_j|}, \ldots, \frac{|v_n|}{\sum_{j=1}^{n}|v_j|}\right]^T.$$

Next, we extract the histogram vector by partitioning the interval $[0, 1]$ into b equal-width bins, where the choice of b depends on the number of vertices in the trees within the dataset.

$$I_k = \left[\frac{k-1}{b}, \frac{k}{b}\right), \quad k = 1, 2, \ldots, b-1$$
$$I_b = \left[\frac{b-1}{b}, 1\right]$$

For each bin k, count the values lies in it:

$$h_k = \sum_{i=1}^{n} \mathbb{I}\left(p_i \in I_k\right)$$

where $\mathbb{I}(\cdot)$ is the indicator function. Then normalize the probability distribution by:

$$\mathbf{h} = \frac{1}{n}[h_1, h_2, \ldots, h_b]^T.$$

thus, $\sum_{k=1}^{b} h_k = 1$.

(4) Concatenate these quantities to form the final feature vector.

The dominant computational cost comes from the eigen-decomposition step, and **the overall time complexity is also** $(O(n^3))$ for a matrix of size $(n \times n)$. For large graphs, this step can be computationally expensive, and more efficient methods or approximations may be required for scalability.

Clustering and Evaluation We apply KMeans to cluster the extracted spectral signatures. The computational complexity of the KMeans algorithm is $O(n \cdot k \cdot d \cdot t)$, where n is the number of samples, k is the number of clusters, d is the dimensionality of the feature space, and t is the number of iterations until convergence. In practice, both the number of clusters and the number of iterations are much smaller than the number of samples, so the algorithm is generally efficient for moderate-sized datasets. However, for very large datasets or high-dimensional data, the computational cost can become significant.

To evaluate performance of clustering, we leverage two widely used metrics.

- Adjusted Rand Index (ARI): Measures agreement with ground truth, corrected for chance.
- Normalized Mutual Information (NMI): Measures mutual dependence between predicted and true labels, normalized to $[0, 1]$.

Method	Metric	Number of Trees (PR/BA/CB)				
		50/50/50	100/100/100	200/200/200	300/300/300	300/200/100
Distance	ARI	0.10 ± 0.03	0.09 ± 0.02	0.09 ± 0.01	0.09 ± 0.01	0.00 ± 0.01
	NMI	0.26 ± 0.03	0.26 ± 0.03	0.25 ± 0.02	0.25 ± 0.01	0.23 ± 0.01
Adjacency	ARI	0.31 ± 0.04	0.31 ± 0.04	0.31 ± 0.02	0.31 ± 0.02	0.40 ± 0.03
	NMI	0.47 ± 0.04	0.47 ± 0.03	0.47 ± 0.02	0.46 ± 0.03	0.49 ± 0.02
Laplacian	ARI	0.23 ± 0.05	0.23 ± 0.04	0.22 ± 0.03	0.22 ± 0.03	0.29 ± 0.03
	NMI	0.40 ± 0.05	0.39 ± 0.04	0.38 ± 0.03	0.38 ± 0.03	0.39 ± 0.03
Evolution	ARI	**0.63 ± 0.17**	**0.56 ± 0.17**	**0.73 ± 0.12**	**0.65 ± 0.16**	**0.69 ± 0.08**
	NMI	**0.66 ± 0.11**	**0.60 ± 0.12**	**0.71 ± 0.09**	**0.66 ± 0.10**	**0.64 ± 0.08**

TABLE 1. Performance comparison across different tree configurations: number of trees sampled from three tree generation models (mean ± std)

Table 5 reports the mean and std of ARI and NMI from 100 runs for different random seeds. In each run, the size of sampled trees varies. For PR and BA trees, nodes number varies in [10, 20, 30, 40, 50, 60, 70, 80, 90, 100], and for CB trees, the depth varies in [5, 6, 7, 8, 9, 10, 11, 12, 13, 14, 15]. The statistic results shows Evolution matrix stably and significantly outperforms other matrices on different scale of datasets. The last column of Table 5 shows even on unbalance datasets, Evolution matrix still show its capability to characterize tree structures.

Figure 7 shows the Multidimensional Scaling (MDS) visualization of tree features extracted from four different matrices. MDS is a dimensionality reduction technique that preserves the distances between features, i.e., if two trees are similar, they appear close in the embedding; if they are very different, they appear far apart. In the first three plots, the clusters are not well separated. Points from different classes often overlap, leading to low ARI and NMI scores. This suggests that Distance, Adjacency, or Laplacian-based features are not sufficient to capture the underlying structural differences among tree types. In contrast, the evolution-based dissimilarity (bottom right) produces a much clearer separation of the three classes. This matrix likely incorporates more meaningful structural features of the trees, capturing their generative process. As a result, Evolution-based features gets the high ARI (0.81) and NMI (0.78).

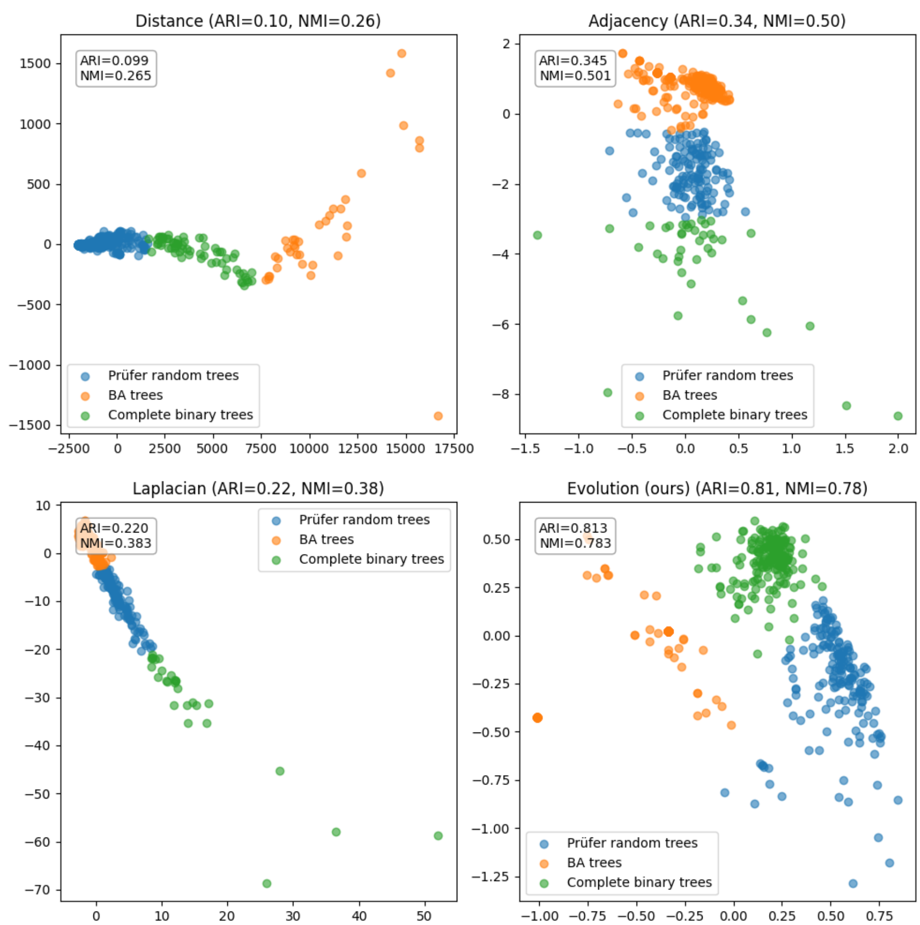

FIGURE 7. MDS visualization of clustering results for different matrix representations. The Evolution Matrix yields the clearest separation among four types.

Experiments show that the Evolution Matrix outperforms adjacency, Laplacian, and distance matrices in clustering accuracy. Based on its construction from the continuous Ricci flow, the Evolution Matrix also exhibits the following design features, which suggest potential advantages beyond our experiments:

(1) *Curvature-aware*: Encodes local geometric information from the Ricci flow.
(2) *Sparse*: Fewer nonzero entries, implying lower computational cost for large trees.

(3) *Interpretable*: Non-zero entries correspond directly to edge–edge interactions.

Why the Evolution Matrix Improves Tree Classification

We now explain, in a geometry–spectral way, why the proposed Evolution Matrix R (Definition 4) yields substantially better clustering of tree topologies than standard choices such as the adjacency, Laplacian, or distance matrices. The key point is that, by construction, *the leading spectral quantities of R related with the limiting geometric objects of the continuous Ricci flow on trees.* Concretely, under our flow,

$$\kappa(\infty) \;=\; -\,\lambda_{\max}(R), \qquad w_\infty \;=\; \mathbf{v}_{\max}(R), \tag{41}$$

where $\kappa(\infty)$ is the limiting curvature, and w_∞ is the normalized Ricci flow metric at equilibrium, while $\lambda_{\max}(R)$ and $\mathbf{v}_{\max}(R)$ denote, respectively, the largest eigenvalue of R and an associated eigenvector. The feature extraction pipeline in §5 naturally extracts the information from (41) (via eigenvalue statistics and the histogram of $|\mathbf{v}_{\max}|$), which aligns the learned representations with the underlying geometry of the data-generating mechanisms.

(R1) Geometry-aligned spectrum (task–feature alignment). Equation (41) shows that the top spectral quantities of R *are* the limiting geometric invariants of the Ricci flow. Hence summary statistics of the spectrum (min/median/max, moments, sign proportions) directly encode the limiting curvature scale and its dispersion, while the normalized histogram of $|\mathbf{v}_{\max}|$ estimates the distribution of the limiting metric across edges. In contrast, for the adjacency A and the Laplacian L, the principal spectral quantities have no direct curvature interpretation; for the distance matrix D_{dist}, eigen-structure is dominated by global path-length geometry and is insensitive to local curvature concentrations. This geometry–spectrum coupling endows R an intrinsic *inductive bias* tailored to separating tree generative models.

(R2) Edge-space, degree-normalized coupling highlights branching geometry. Indexing R by edges (not vertices) and using $1/d_v$ couplings at each endpoint causes R to emphasize how edges *share* branching load at high-degree vertices. For an edge $e = \{x, y\}$,

$$R_{e,e} \;=\; -\Big(\tfrac{1}{d_x} + \tfrac{1}{d_y}\Big), \qquad R_{e,e'} \;=\; \begin{cases} \tfrac{1}{d_x}, & e \cap e' = \{x\}, \\ \tfrac{1}{d_y}, & e \cap e' = \{y\}, \\ 0, & \text{otherwise.} \end{cases}$$

Thus, edges incident to hubs (large d) experience a characteristic pattern of many small $1/d$ -strength couplings whose global superposition yields a distinctive leading eigenvector footprint:

- **BA trees (heavy-tailed degrees):** mass in $|\mathbf{v}_{\max}|$ concentrates around hub-incident edges; the histogram of $|\mathbf{v}_{\max}|$ displays heavier upper-bin occupancy.
- **Complete binary trees (regular, hierarchical):** near-uniform degree induces a smoother, more homogeneous $|\mathbf{v}_{\max}|$ -histogram.
- **Prüfer random trees (light-tailed degrees):** patterns lie between the two extremes, with moderate concentration.

The same mechanism also affects $\lambda_{\max}(R)$, hence curvature scale, yielding class-separable statistics without requiring large feature engineering.

(R3) Scale robustness induced by $1/d$ -normalization. Because the couplings at a vertex are normalized by the local degree, R attenuates the raw effect of graph size and emphasizes *relative branching proportions*. When node counts or depths vary across samples (as in our setup), the eigenvalue moments and $|\mathbf{v}_{\max}|$ -histograms remain comparably distributed within a model class. By contrast, D_{dist} -spectra drift substantially with size (global path lengths stretch), while A and L are more sensitive to absolute degree counts than to their *normalized* branching structure.
(R4) Line-graph viewpoint: as a Laplacian-type operator on edges. Let $\mathcal{L}(T)$ be the line graph of T (its vertices are edges of T). If one forms a weighted Laplacian on $\mathcal{L}(T)$ with weights $w(e, e') = 1/d_v$ whenever e and e' meet at v, then R can be seen as a *Laplacian-like* operator on edge space, up to a degree-dependent diagonal shift (sign conventions reversed on off-diagonals). This places R squarely in the class of *diffusion generators* on edge functions, which mirrors the curvature-smoothing nature of the Ricci flow. The adjacency A and vertex-Laplacian L act on different state spaces (nodes rather than edges) and do not implement this particular curvature-aware diffusion.
(R5) Why the chosen features are especially effective for R. Our pipeline (§5) uses (i) eigenvalue summary statistics and (ii) a histogram of the normalized leading eigenvector. For R, these two blocks *exactly* probe the quantities in (41):

(1) The statistics of $\{\lambda_i(R)\}$ summarize the curvature scale and its dispersion across modes (mean/variance/skew/kurtosis; proportions of signs).
(2) The histogram of $|\mathbf{v}_{\max}(R)|$ summarizes how the limiting Ricci metric m_∞ distributes over edges (concentration vs. spread), which is highly diagnostic of hub-dominated vs. regular branching.

Applying the *same* feature recipe to A, L, and D_{dist} produces descriptors that lack this geometric semantics; consequently, the resulting embeddings are less aligned with the differences induced by the generative models and thus less separable for clustering.
(R6) Testable predictions and ablations. The geometric reading above yields empirical predictions that further explain the observed gains:

- *Ablation:* Using only $\lambda_{\max}(R)$ plus the $|\mathbf{v}_{\max}(R)|$ -histogram should retain most of the performance, since these already capture curvature scale and limiting metric concentration.
- *Local perturbations:* Edge operations that change branching at a hub (adding/removing multiple leaves at a high-degree vertex) should cause a larger, more structured drift in R -spectra than in the spectra of A, L, or D_{dist}, matching geometric intuition.
- *Size extrapolation:* Within a fixed model class, as n grows, the empirical distribution of $|\mathbf{v}_{\max}(R)|$ -histograms should stabilize (after appropriate binning), whereas D_{dist} -based summaries drift with graph diameter.

The Evolution Matrix R embeds the continuous Ricci flow's limiting curvature and metric *directly* into its leading spectral data. Because the differences among

BA/Prüfer/complete-binary trees are fundamentally expressed by their branching geometry (hub concentration vs. regularity), the geometry-aligned spectrum of R produces features that are both interpretable and strongly discriminative, thereby explaining its superior clustering accuracy in our experiments.

6. Future Work

In the previous section, we observed that the Ricci flow matrix exhibits promising potential for distinguishing trees through their spectra and the eigenvector. A natural question that arises is whether the largest eigenvalue and the eigenvector can serve as a complete invariant for finite trees, as suggested by Conjecture 1. At present, this remains an open problem, and we leave a rigorous investigation of this conjecture for future research.

Conjecture 1 (Spectral Rigidity via the Leading Eigenpair)**.** *Let T_1 and T_2 be finite, connected, undirected trees, and let R_{T_1} and R_{T_2} denote their Ricci flow matrices. Suppose the largest eigenvalues and corresponding eigenvectors coincide:*

$$\lambda_{\max}(R_{T_1}) = \lambda_{\max}(R_{T_2}), \quad v_{\max}(R_{T_1}) = v_{\max}(R_{T_2}) \ \text{(up to scaling)}.$$

Then the trees are isomorphic:

$$T_1 \cong T_2.$$

References

[1] Shuliang Bai, An Huang, Linyuan Lu, and Shing-Tung Yau. On the sum of ricci-curvatures for weighted graphs. *Pure and Applied Mathematics Quarterly*, 17(5):1599–1617, 2021.

[2] Shuliang Bai, Yong Lin, Linyuan Lu, Zhiyu Wang, and Shing-Tung Yau. Ollivier ricci-flow on weighted graphs. *American Journal of Mathematics*, 146(4), 2024.

[3] Bennett Chow and Feng Luo. Combinatorial Ricci Flows on Surfaces. *Journal of Differential Geometry*, 63(1):97–129, 2003.

[4] David Cushing, Supanat Kamtue, Shiping Liu, Florentin Münch, Norbert Peyerimhoff, and Hugo Benedict Snodgrass. Bakry–Émery curvature sharpness and curvature flow in finite weighted graphs: Implementation. *Axioms*, 12(6):577, 2023.

[5] Matthias Erbar and Eva Kopfer. Super ricci flows for weighted graphs. *Journal of Functional Analysis*, 279(6):108607, 2020.

[6] Ke Feng, Huabin Ge, and Bobo Hua. Combinatorial Ricci flows and the hyperbolization of a class of compact 3–manifolds. *Geometry & Topology*, 26(3):1349–1384, 2022.

[7] Huabin Ge. Combinatorial calabi flows on surfaces. *Transactions of the American Mathematical Society*, 370(2):1377–1391, 2018.

[8] Huabin Ge, Bobo Hua, and Ze Zhou. Circle patterns on surfaces of finite topological type. *American Journal of Mathematics*, 143(5):1397–1430, 2021.

[9] David Glickenstein. A combinatorial yamabe flow in three dimensions. *Topology*, 44(4):791–808, 2005.

[10] David Alan Glickenstein. *Precompactness of the Ricci flow and a maximum principle on combinatorial Yamabe flow*. ProQuest LLC, Ann Arbor, MI, 2003. Thesis (Ph.D.)–University of California, San Diego.

[11] Xianfeng David Gu, Feng Luo, Jian Sun, and Tianqi Wu. A discrete uniformization theorem for polyhedral surfaces. *Journal of Differential Geometry*, 109(2):223–256, 2018.

[12] Richard Hamilton. Three-manifolds with positive ricci curvature. *Journal of Differential Geometry*, 17:255–362, 06 1982.

[13] Richard Hamilton. Four-manifolds with positive curvature operator. *Journal of Differential Geometry*, 24(2):153–179, 1986.

[14] Richard S. Hamilton. The ricci flow on surfaces. *Mathematics and General Relativity, Contemp. Math.*, 71:237–262, 1988.

[15] Bobo Hua, Yong Lin, and Tao Wang. A version of bakry-Émery ricci flow on a finite graph. *arXiv*, arXiv:2402.07475, 2024.

[16] Miao Jin, Junho Kim, and Xianfeng David Gu. Discrete surface ricci flow: Theory and applications. In Ralph Martin, Malcolm Sabin, and Joab Winkler, editors, *Mathematics of Surfaces XII*, pages 209–232, Berlin, Heidelberg, 2007. Springer Berlin Heidelberg.

[17] Ruowei Li and Florentin Münch. The convergence and uniqueness of a discrete-time nonlinear markov chain. *arXiv preprint arXiv:2407.00314*, 2025.

[18] Yujia Li, Daniel Tarlow, Marc Brockschmidt, and Richard Zemel. Gated graph sequence neural networks. In *Proceedings of ICLR*, 2015.

[19] Yong Lin, Linyuan Lu, and Shing-Tung Yau. Ricci curvature of graphs. *Tohoku Mathematical Journal*, 63, 12 2011.

[20] Christopher D. Manning and Hinrich Schütze. *Foundations of Statistical Natural Language Processing*. MIT Press, 1999.

[21] Chien-Chun Ni, Yu-Yao Lin, Jie Gao, and Xianfeng David Gu. Network alignment by discrete ollivier-ricci flow. *Graph Drawing and Network Visualization*, 11282:447–462, 2018.

[22] Chien-Chun Ni, Yu-Yao Lin, Feng Luo, and Jie Gao. Community detection on networks with ricci flow. *Scientific Reports*, 9, 07 2019.

[23] Joakim Nivre. Dependency grammar and dependency parsing. In *MSR Workshop on Treebanks and Linguistic Theories*, 2005.

[24] Grigori Perelman. The entropy formula for the ricci flow and its geometric applications, 2002.

[25] Grigori Perelman. Finite extinction time for the solutions to the ricci flow on certain three-manifolds, 2003.

[26] Grigori Perelman. Ricci flow with surgery on three-manifolds, 2003.

[27] Richard Socher, Alexey Perelygin, Jean Y. Wu, Jason Chuang, Christopher D. Manning, Andrew Ng, and Christopher Potts. Recursive deep models for semantic compositionality over a sentiment treebank. In *Proceedings of the 2013 Conference on Empirical Methods in Natural Language Processing (EMNLP)*, pages 1631–1642, 2013.

[28] Jake Topping, Francesco Di Giovanni, Benjamin Paul Chamberlain, Xiaowen Dong, and Michael M. Bronstein. Understanding over-squashing and bottlenecks on graphs via curvature. In *International Conference on Learning Representations*, 2022.

[29] Melanie Weber, Jürgen Jost, and Emil Saucan. Forman-ricci flow for change detection in large dynamic data sets. *Axioms*, 5(4), 2016.

[30] Melanie Weber, Emil Saucan, and Jürgen Jost. Characterizing complex networks with forman-ricci curvature and associated geometric flows. *Journal of Complex Networks*, 5(4):527–550, 01 2017.

[31] Min Zhang, Ren Guo, Wei Zeng, Feng Luo, Shing-Tung Yau, and Xianfeng Gu. The unified discrete surface ricci flow. *Graphical Models*, 76(5):321–339, 2014. Geometric Modeling and Processing 2014.